Title

Advances in remote sensing techniques for monitoring and predicting plant physiology and biochemistry

Author

Brissette, Logan E.G.

Publication Date

2023

Peer reviewed|Thesis/dissertation

Advances in remote sensing techniques for monitoring and predicting plant physiology and biochemistry

By

LOGAN E. G. BRISSETTE
THESIS

Submitted in partial satisfaction of the requirements for the degree of

MASTER OF SCIENCE

in

Ecology

in the

OFFICE OF GRADUATE STUDIES

of the

UNIVERSITY OF CALIFORNIA

DAVIS

Approved:

Troy Magney, Chair

Matthew Gilbert

Barry Logan

Committee in Charge

2023

To my cherished, chosen, and collected family, and to all those who have supported me throughout the years,
especially Evan, Tramp, Jeeves, Teddy, Watson,
and Troy.

Abstract

This thesis investigates novel remote sensing approaches to monitor and predict plant physiology and biochemistry in response to environmental stressors and seasonal changes. Divided into two chapters, each explores a distinct remote sensing technique and its application in understanding the connection between plant physiology and remote sensing.

Chapter 1 introduces a novel nighttime low-cost photodiode method, which was tested during a drought response experiment of LED-induced canopy-level chlorophyll *a* fluorescence (LEDIF) in *Polygala myrtifolia*. Far-red LEDIF (720 - 740 nm) was retrieved using low-cost photodiodes ($LEDIF_{photodiode}$) and a hyperspectral instrument ($LEDIF_{hyperspectral}$). To link the LEDIF signal with physiological drought response, we tracked stomatal conductance (g_{sw}) using a porometer as an indicator of plant water status, two leaf-level vegetation indices — photochemical reflectance index, PRI; normalized difference vegetation index, NDVI— to represent chlorophylls and xanthophyll pigment dynamics, respectively, and a pulse-amplitude modulation (PAM) device to measure photochemical and non-photochemical dynamics of photochemistry. Our results demonstrate a similar performance between the photodiode and hyperspectral retrievals of LEDIF ($R^2=0.77, P < 0.01$). Furthermore, $LEDIF_{photodiode}$ closely tracked drought responses with photochemical quenching (PQ, $R^2=0.69, P < 0.001$), Fv/Fm ($R^2=0.59, P < 0.001$), and leaf-level PRI ($R^2= 0.59, P<0.05$). The results demonstrate the potential of this cost-effective method to accurately track changes in photosynthetic status and overall plant health, offering valuable insights into the relationships between the physiological mechanisms of photosynthesis and chlorophyll fluorescence.

Chapter 2 employs hyperspectral reflectance data to predict an array of chlorophyll and carotenoid pigment concentrations in *Pinus palustris* (Longleaf Pine) using a partial least squares regression modeling approach. This study took place in north-central Florida, at the Ordway Swisher Biological Station (OSBS), and more specifically, the National Ecological Observation Network (NEON) flux tower site within it. The research site is dominated by mature Longleaf Pines and low-lying perennial grasses. From six Longleaf Pine trees, branches were harvested, and needles were either 1) immediately stored for later pigment extraction and 2) made into needle mats to retrieve reflectance measurements with our hyperspectral spectroradiometer's leaf clip. Needle mats were assembled by laying individual needles flat and continuously side by side until they were approximately 5-6 cm wide, and were held together by two pieces of tape, arranged at the top and bottom of the needles. Using a PLSR modeling approach, our prediction task for each PLSR model was to predict the average pigment content of a tree, using a hyperspectral reflectance measurement of a single needle mat (for each pigment/pool) per tree. Our results reveal the potential of hyperspectral remote sensing to estimate plant pigments accurately and efficiently; our PLSR models successfully predicted the concentrations with R^2 values > 50% for eight of the ten pigments/pools. We were able to best predict lutein and neoxanthin, as well as chlorophyll *b* and *a* ($R^2 = 0.91$, $RMSE = 0.01$; $R^2 = 0.77$, $RMSE = 0.0$; $R^2 = 0.68$, $RMSE = 0.02$; $R^2 = 0.65$, $RMSE = 0.05$, respectively). This research demonstrates the value of leaf-level remote sensing in advancing our understanding of the physiological status of evergreen species and their underlying pigments.

Collectively, these chapters showcase the power of remote sensing for monitoring and predicting plant responses to environmental stressors and seasonal changes. They offer valuable insights into the relationships between plant physiology and remote sensing, paving the way for improved strategies to assess plant health and resilience in the face of changing environmental conditions.

Contents

1 Tracking the short-term drought response of canopy chlorophyll fluorescence with a low-cost nighttime LED platform

Logan E.G. Brissette, Chris Y.S. Wong, Erica Orcutt, Devin McHugh, and Troy S. Magney

1.1 Abstract

Chlorophyll fluorescence measured at the leaf scale through pulse amplitude modulation has provided invaluable insight into photosynthesis. At the canopy- and satellite-scale, solar-induced fluorescence (SIF) has revealed a method to estimate the photosynthetic activity of plants across spatiotemporal scales. However, retrieving the chlorophyll fluorescence signal remotely requires instruments with high spectral resolutions, making it difficult and often expensive to measure canopy-level steady-state chlorophyll fluorescence under natural sunlight.

In light of this, we sought to build a novel low-cost photodiode system that retrieves far-red chlorophyll fluorescence emissions induced by a blue light emitting diode (LED) light-source, for two hours at night, above the canopy. Our objective was to determine if our active remote sensing nighttime photodiode method could track changes in canopy-scale LED-induced chlorophyll fluorescence (LEDIF) during an imposed drought on a broadleaf evergreen shrub, *Polygala myrtifolia*. Far-red LEDIF (720 - 740 nm) was retrieved using low-cost photodiodes ($LEDIF_{photodiode}$) and a hyperspectral instrument ($LEDIF_{hyperspectral}$). To link the LEDIF signal

with physiological drought response, we tracked stomatal conductance (g_{sw}) using a porometer as an indicator of plant water status, two leaf-level vegetation indices — photochemical reflectance index, PRI; normalized difference vegetation index, NDVI— to represent xanthophyll and chlorophyll pigment dynamics, respectively, and a pulse-amplitude modulation (PAM) device to measure photochemical and non-photochemical dynamics of photochemistry. Our results demonstrate a similar performance between the photodiode and hyperspectral retrievals of LEDIF ($R^2=0.77, P < 0.01$). Furthermore, $LEDIF_{photodiode}$ closely tracked drought responses with photochemical quenching (PQ, $R^2=0.69, P < 0.001$), Fv/Fm ($R^2=0.59, P < 0.001$), and leaf-level PRI ($R^2= 0.59, P<0.05$). Therefore, $LEDIF_{photodiode}$ has the potential to be a meaningful indicator of photosynthetic activity, and thus, overall plant "health". Moreover, because of its cost-effective nature (hundreds versus thousands of dollars), this method may allow for more equitable, repeatable validation experiments to be performed in a variety of systems, further elucidating the relationships between the physiological mechanisms of photosynthesis and chlorophyll fluorescence.

1.2 Introduction

The terrestrial biosphere acts as a crucial sink for current and future atmospheric CO_2 through the process of photosynthesis (Turner et al. 2006; Beer et al. 2010; Ryu et al. 2019). Although photosynthesis can be more directly measured at the leaf-level, scaling estimates of photosynthesis to canopy- and ecosystem-level can be labor or model intensive, expensive, and requires specialized equipment (Baldocchi 2003; Ryu et al. 2019; Sun et al. 2019). Fortunately, remote sensing technologies have been developed to aid in large scale estimates of

photosynthesis, allowing us to better scale gross primary productivity (GPP) globally (Sun et al. 2018 *a*; Xiao et al. 2019; Ryu et al. 2019). Despite the promise of satellite-based estimates of GPP, global carbon cycle uncertainty remains high (Xiao et al. 2019; Zhang and Ye, 2021). This is because satellite-data remain difficult to interpret without a mechanistic understanding of when, why and to what extent reflected or re-emitted photons co-vary with changes in photosynthesis. To aid in this, having a network of remote sensing technologies at a variety of scales— satellites, airborne, tower, leaf— linked with plant physiological measurements, can provide invaluable insight into the temporal dynamics of plant function.

Reflectance-based vegetation indices (VIs) have been used to estimate GPP (Peng et al. 2011; Lin et al. 2019; Huang et al. 2019), but performance may be limited in certain scenarios (Xue and Su, 2017). One of the most well-known VIs is the normalized difference vegetation index — NDVI, which estimates vegetation 'greenness' and used to infer the health and productivity of the plants (Tucker 1979). However, NDVI may saturate in areas of dense vegetation (i.e., high leaf area index), such as croplands and forested areas (Baret and Guyot 1991; Huete et al. 1997; Sun et al. 2018 *b*). Furthermore, as NDVI is a metric of green plant biomass, it may be limited in assessing photosynthetic activity in ecosystems with little structural change, such as evergreen dominated ecosystems (Magney et al. 2019; Pierrat et al. 2022). As a result, physiologically sensitive VIs may provide an advantage for monitoring vegetation function; such as the photochemical reflectance index (PRI, Gamon et al. 1992). PRI changes rapidly under increasing incident light as excess energy builds due to saturating photochemistry, leading to de-epoxidation of xanthophyll cycle pigments (a subgroup of carotenoids) —violaxanthin into the photoprotective antheraxanthin and zeaxanthin— to dissipate the excess energy (Demmig-

Adams and Adams 1996; Gamon et al. 1997). Thus, PRI can track fluctuations in photoprotective carotenoid pigment activity, which can then be used as a proxy for daily or even seasonal changes in photosynthetic activity (Garbulsky et al. 2011; Magney et al. 2016; Pierrat et al. 2022), and as an early indicator of plant stress from environmental changes such as drought (Magney et al. 2016; Sarlikioti et al. 2010; Zhang et al. 2017).

Vegetation indices have demonstrated that we can use remote sensing proxies to inform our understanding of changes in plant 'greenness' and pigments (Glenn et al. 2008); however, we can further probe photosynthetic activity by understanding and measuring the fate of photons upon reaching the leaf. Inside the leaf, there are three dominant competing pathways in which absorbed light energy can be quenched by the plant. Absorbed light energy can be 1) used for photochemistry (aka photosynthesis), 2) emitted as fluorescence, or 3) dissipated as heat — non-photochemical quenching (NPQ, Murchie and Lawson 2013; Porcar-Castell et al. 2014).
As the three pathways are in competition—meaning that an increase in one may result in a decrease in the other pathways—measuring chlorophyll fluorescence can enable inference into the dynamics of photochemistry and NPQ (Maxwell and Johnson 2000; Baker 2008; Magney et. al 2017).

Chlorophyll *a* fluorescence has been actively measured at the leaf-level through pulse amplitude modulation (PAM) fluorometry for decades (Baker and Oxborough, 2004). The natural progression of fluorescence research, then, has been to scale leaf-level PAM measurements to the canopy-level spectral fluorescence emissions (Mohammed et al. 2019; Porcar-Castell et al. 2021). For over a decade now, solar-induced fluorescence (SIF), measured from 650-850 nm,

has been used to measure chlorophyll fluorescence passively through satellites (Frankenberg et al. 2011; Joiner et al. 2011). SIF is measured as a red-far-red glow in the Fraunhofer lines (Frankenberg et al. 2011; Joiner et al. 2011), but it has also been quantified using the oxygen bands (Meroni et al. 2009). Further investigation of SIF has shown a linear relationship between SIF and GPP at the satellite-level (Sun et al. 2017, 2018 *a*). This is promising; however, there are considerations to making SIF measurements during the daytime. To measure SIF under natural sunlight, expensive, highly sensitive spectrometers are necessary to resolve the Fraunhofer lines (Grossmann et al. 2018). Moreover, SIF is also highly dynamic and represents the state of a plant during the current environmental conditions such as water availability, temperature, vapor-pressure deficit, or light intensity (Verma et al. 2017; Magney et al. 2019). Additionally, further investigation of the relationship between SIF and GPP is necessary at smaller spatial- and temporal-scales, and across all ecosystems (Porcar-Castell et al. 2021). Therefore, specifically investigating the relationship between leaf and canopy fluorescence with photosynthesis, especially under stress events like drought, may provide novel insight into the connection of physiology and remote sensing proxies.

Detecting drought is becoming increasingly important, as droughts are becoming more frequent, widespread, and intense (Allen et al. 2010; Chiang et al. 2021). The effects of drought on plants have been laboriously measured via changes in stomatal conductance (Wu et al. 2019), cavitation (Vilagrosa et al. 2003; Choat et al. 2012; Fichot et al. 2015), as well as through remote sensing proxies such as VIs (Wagle et al. 2014; Rousta et al. 2020). SIF, with its inherent connection to the competing pathways of absorbed light, allows stress detection to happen before any visible signs in leaf coloration (Magney et al. 2020; Kimm et al. 2021). However, the nuances of how

SIF changes under drought stress have not been thoroughly studied. Flexas et al. (2002 *a, b*) showed that an increase in drought stress caused a series of physiological changes in the plant, including an increase in NPQ, a decrease in photochemical quenching, and a non-linear decrease in steady-state fluorescence emission; which could lead to a change in the relationship of SIF and carbon uptake. Interestingly, when looking into the leaf level relationship between fluorescence and photosynthesis during a short-term drought, Helm et al. (2020) found that chlorophyll *a* fluorescence did not reflect a strong response to drought, yet the response was strongly observed in the stomata and rate of photosynthesis. A better understanding of how SIF changes in response to stress at the leaf- and canopy-level is essential for interpretation of SIF data to estimate carbon fluxes across various environments.

Expanding on the fluorescence research and relationships established through PAM and SIF, light-emitting diodes (LEDs) have been employed at night to actively measure canopy-level chlorophyll *a* fluorescence. Romero et al. (2018) successfully used LEDs to measure and model canopy fluorescence and calculate reabsorption values in a controlled plant canopy environment. In a forest consisting of Scots Pine and lingonberry, a colored (blue, red, and green) LED system was installed above the canopies and illuminated the canopy for two hours (Atherton et al. 2019). In this study, using a field spectrometer at night with long integration times, they measured the quantum yield of fluorescence excited by the LED lights (red, green, and blue) and coined the new nocturnal method: LED-Induced chlorophyll *a* Fluorescence— LEDIF (Atherton et al. 2019). Romero et al. (2021) built an LEDIF system and implemented it in an agricultural environment. They investigated how aerial net primary productivity varied with different water treatments and bean cultivars using passive (VIs, PAM, and SIF) and active (LEDIF) remote

sensing to discern changes in plant health. They found that chlorophyll *a* fluorescence, whether collected passively or actively, proffered insight into plant health before any visible cues. These studies are encouraging because of their ability to detect physiological changes and give warning signs of plant stress. However, a common theme across these research investigations is that measuring fluorescence at night was done using a spectrometer, which prohibits low-cost applications. Because these measurements were done at night, a lower cost spectrometer (several thousand dollars) can be used because spectral resolution is not an issue.

Our nighttime LED system is unlike current self-built daytime SIF measuring systems, such as PhotoSpec (Grossman et al. 2018) and FluoSpec (Yang et al. 2015, 2018), which require thermally stable, high spectral resolution spectrometers (tens of thousands of dollars). To address this, we developed a simple, repeatable, easy to install, financially equitable alternative to measuring chlorophyll *a* fluorescence. We measured chlorophyll fluorescence at night using a blue LED light source, which offered the potential to measure a pure fluorescence signal using low-cost photodiodes (hundreds of dollars) in the far-red region. Therefore, our objectives were 1) to determine if we can track changes in canopy-level chlorophyll fluorescence with a new, nighttime, low-cost sensor during an imposed stress event and 2) investigate whether these changes are reflected at the leaf- and canopy-level. To accomplish this, we compared the temporal dynamics of LEDIF from our inexpensive photodiode system to that of a more expensive hyperspectral spectrometer. We investigated the relationship between the physiological and fluorescence parameters to contextualize and understand how our platform performed against more traditional methods. An effective, labor-reducing, low-cost LEDIF platform will more readily allow for implementation into a variety of systems that will shed even

more light into the physiological mechanisms linking chlorophyll fluorescence and photosynthesis at the leaf-level.

1.3 Methods and materials

1.3.1 Experimental setup

Sweet Pea Shrub (*Polygala myrtifolia*), an ornamental evergreen shrub species, was selected for this study. The plant was fully established at a local greenhouse in Davis, California, and was acquired mid-March 2021. We initiated a controlled drought and recovery experiment in early spring that began on April 5th, 2021, and lasted for 25 days. Our experiment consisted of three periods: pre-drought: April 5th - April 16th where the plant was well-watered, drought: April 17th - April 23rd where the plant was completely unwatered, and post-drought: April 24th – April 29th where we began watering regularly again (Table 1.1).

The experiment took place in a wood-built structure (Fig. 1.1), on an experimental plot located in northern Davis, California. Excessive shading by the structure was avoided by cutting large windows in the top panel of the structure. These windows did not interfere with the solar panels that powered the MONI-PAM, or with the ceiling mounted photodiode radiometers and lights. Five blue LED lights (three @ 5 Watts and two @ 15 Watts) were mounted ~20 cm above the canopy (FZWLE RGBW 5W LED Spot Lights; Pesken Lighting RGB+CW 15W Flood Lights). Measured PAR values at the top of the canopy ranged from 15-30 umol m-2 s-1, inducing a light level equivalent to minimal fluorescence (F_o) from PAM. The lights were positioned around the photodiode sensor, in a circular arrangement that enclosed but did not touch the sensor and

ensured that the top of the canopy was fully illuminated. Extraneous light from surrounding plots was blocked by a heavy-duty tarp placed around the housing structure and was secured to the ground on each side from dusk until dawn, each day. After at least 15 minutes of being completely shaded under the tarp, the LEDs were then switched on for 2 hours, nightly, starting no earlier than 2030h and no later than 2130h. The LEDs provided the irradiance necessary to actively measure nighttime fluorescence in *P. myrtifolia* (Fig. 1.2a).

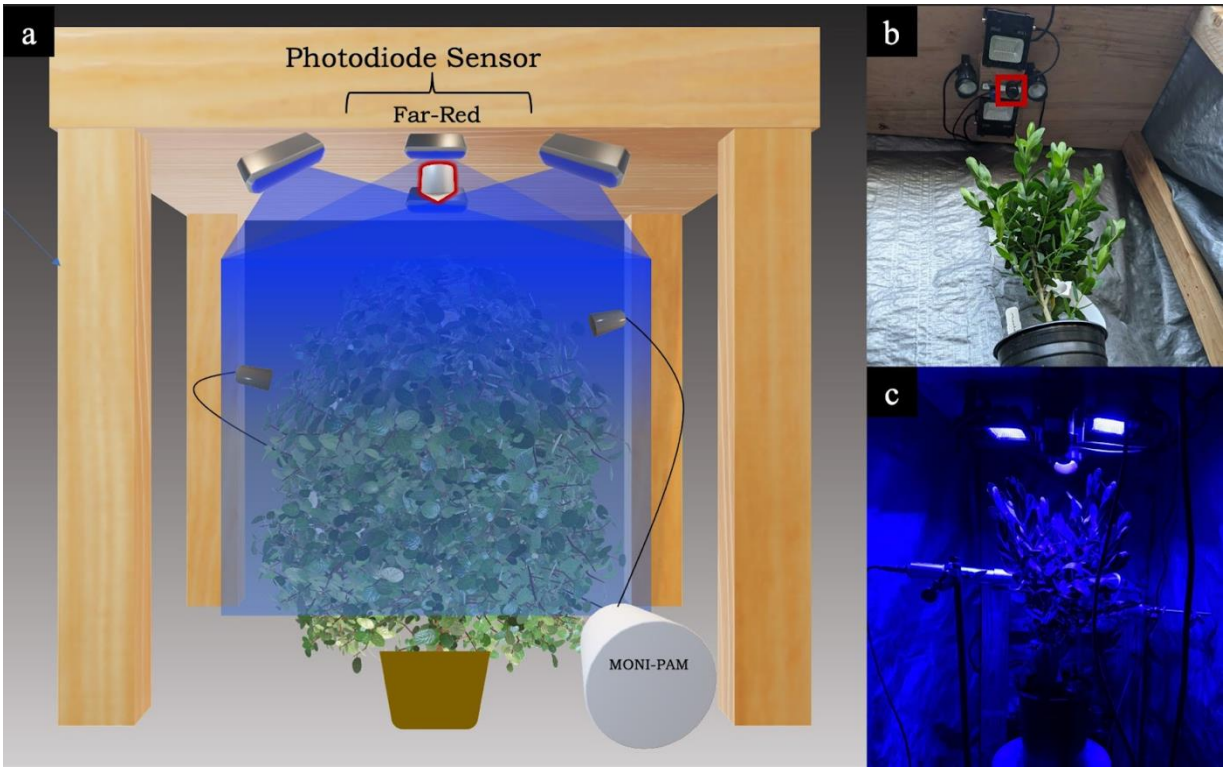

Figure 1.1 : a) Conceptual figure showing the setup and layout for novel LEDIF drought experiment. b) View of built structure with mounted LED lights encircling the photodiode radiometer sensor (sensor outlined in red). c) View of setup with blue LEDs on, sensors connected (photodiode: above, MONI-PAM: heads attached to leaves mid-canopy), and tarp excluding extraneous environmental lighting.

1.3.2 Canopy-Level Measurements

1.3.2.1 *Broadband photodiode radiometer*

A photodiode radiometer, measuring in the red/far-red regions (645 nm to 665 nm, 720 nm-740 nm, respectively) with a FOV of 180°, was mounted ~20 cm from the top of the canopy (S2-131, Apogee Instruments, Inc, Logan, Utah, USA). This relatively inexpensive sensor (~$250/sensor) provided continuous spectral measurements throughout the duration of the experiment. Data were logged every five minutes, throughout each day. Data collection started on April 10th, 2021 and were stored on data loggers and downloaded regularly (AT-100 microCache Bluetooth Micro Logger, Apogee Instruments, Inc, Logan, Utah, USA) (Table 1.1). Ultimately these data were used to quantify steady-state chlorophyll *a* fluorescence emission, in the far-red region. Data collected in the red region (645 nm to 665 nm) were not used as this range was outside of the fluorescence emission that was excited by the blue LEDs (Fig. 1.2b).

Table 1.1. shows the timing of when data were taken, each instrument was used, and what data were collected. Numbers reference dates in April, 2021: i.e. "5" is the 5th of April, 2021. Blue text refers to canopy-level measurements and green text refers to leaf-level measurements. Shaded regions indicate watering period: green= pre-drought, brown= drought, purple= post-drought.

		Study Timeline (April 2021)																								
Instrument & Parameter		**5**	**6**	**7**	**8**	**9**	**10**	**11**	**12**	**13**	**14**	**15**	**16**	**17**	**18**	**19**	**20**	**21**	**22**	**23**	**24**	**25**	**26**	**27**	**28**	**29**
Apogee Photodiode Radiometer	$LEDIF_{photodiode}$	X	X	X	X	X	X	X	X	X	X	X	X	X	X	X	X	X	X	X	X	X	X	X	X	X
SVC Hyperspectral Spectroradiometer	$LEDIF_{hyperspectral}$ NDVI PRI	X		X		X		X		X		X		X		X		X	X		X	X		X		
Li600 Porometer/Fluorometer	g_{sw}	X	X	X	X	X	X	X	X	X	X	X			X	X	X	X	X	X		X	X	X	X	X
MONI-PAM Fluorometer	F_o` PQ NPQ F_V/F_M	X	X	X	X	X	X	X	X	X	X	X	X	X	X	X	X	X	X	X	X	X*	X	X	X	X

Far-red values were summarized (daily mean and standard deviation) across the active LED light period (Fig. 1.2a). One hour after the LED lights were turned off, these metrics were again summarized over a 1-hour period, to get the 'dark period' values. For example, in Figure 1.2a, the tarp was placed at 2021h, the blue LEDs were turned on at 2041h, and then were turned off at 2241h. For the dark period measurements, the average over 2341h until 0041h was taken. In this study, steady-state fluorescence values were gathered from the far-red region (720 nm-740 nm) and will henceforth be referred to as $LEDIF_{photodiode}$ (Fig. 1.2b). $LEDIF_{photodiode}$ have also been dark corrected; dark period values were subtracted from the LED light period values, for each day during the experiment, to get the dark corrected values used in all analysis and figures.

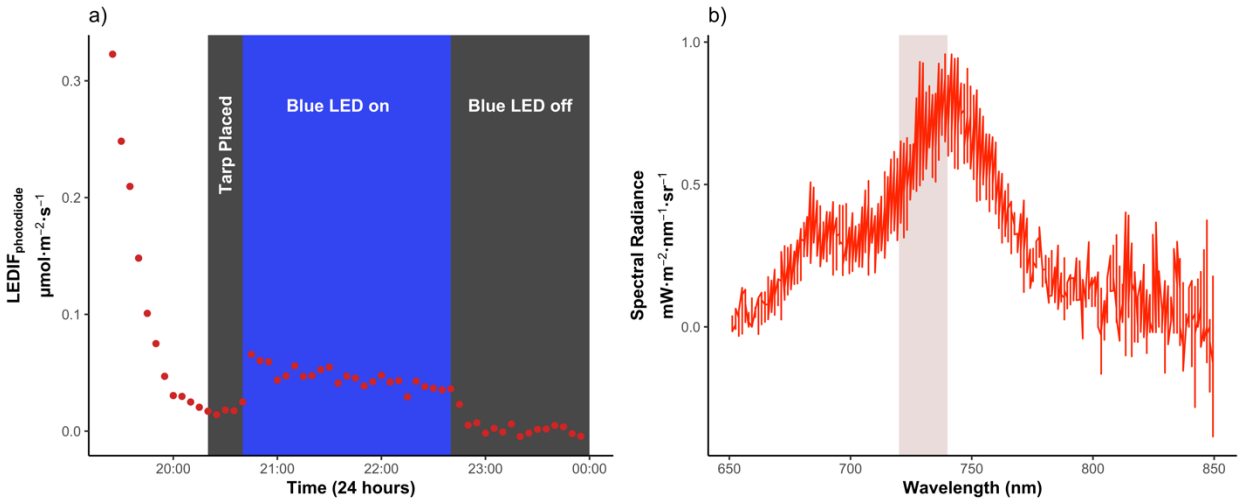

Figure 1.2: a) Displays the $LEDIF_{photodiode}$ canopy-level chlorophyll *a* fluorescence immediately before, during, and after the blue LED lights are turned on and off. A tarp is placed over the platform to prevent an extra light from entering the measurement area for at least 15 minutes prior to the LEDs being turned on. The blue LEDs are then switched on for a 2-hour period. An hour AFTER the blue LEDs are switched

off, the “dark-period” far-red region spectra are then taken, averaged over the following hour period. $LEDIF_{photodiode}$ values are corrected using the averaged “dark-period” values. b) displays the chlorophyll *a* fluorescence emission spectrum collected from the hyperspectral spectrometer during the “blue LED on” period . The shaded region indicated the wavelengths being measured with the far-red photodiode sensor (720 nm-740 nm).

1.3.2.2 *Field hyperspectral spectroradiometer*

LED-induced steady-state canopy fluorescence ($LEDIF_{hyperspectral}$) was measured using a hyperspectral spectroradiometer (HR-1024i, Spectra Vista Corporation, Poughkeepsie, New York, USA). The specifications on this spectroradiometer were a 25° FOV optic fiber and an integration time of 1s. Measurements were taken approximately every other day during the pre- and post-drought periods, while more frequent measurements were taken during the latter half of the induced drought period (Table 1.1). After the lights were activated, a period of 15 minutes was given before measurements started, allowing the plant to adjust to the new light source and avoid the Kautsky effect (Kautsky and Hirsch 1931; Lichtenthaler 1992) (Fig. 1.2a). Note that a tarp stayed over the structure while the nighttime sampling occurred to block any extraneous light from entering. A single canopy average was obtained by repeating a series of four scans taken every 90° around the plant, with the fiber head at an angle of 45° and ~15 cm above the top of the canopy, each day that measurements were made.

These canopy fluorescence measurements were made to have a direct comparison of those collected from our new inexpensive photodiode sensor platform system. In order to make this comparison as appropriate as possible, fluorescence values collected from the hyperspectral

spectroradiometer were averaged over the same wavelengths to the broadband photodiode sensors (720 nm - 740 nm). Daily canopy averages of emitted radiance in this region were then averaged over the 4 scans (Fig. 1.2b).

1.3.3 Leaf-level Measurements

1.3.3.1 *Pulse amplitude modulated fluorescence*

At the leaf-level, active fluorescence measurements were taken using a MONITORING-PAM device (MONI-PAM, Heinz Walz GmbH, Effeltrich, Germany). Two measuring head clips were attached to two randomly chosen leaves. Measuring light intensity was set at 1.5-22 μmol $m^{-2}s^{-1}$ at 100 Hz modulating frequency. The saturation pulse used was 8500 μmol $m^{-2}s^{-1}$ for 0.6 s.

A series of leaf-level metrics were calculated from data collected by the MONI-PAM. Initial parameters collected and descriptions are included in Table 1.2 (adapted from Baker 2008). The MONI-PAM took measurements continuously (24 hr/day) for the duration of the experiment, but logged data every half-hour. Nighttime values were values parsed from data collected between 0000h and 0500h (i.e. F_m, F_o). Daytime values were parsed from data collected between 1100h to 1600h (i.e. F_m', F_s, F_o'). Daily averages (across both measuring heads and day/night hours specified) were then taken to match other instrumentation for the best comparisons possible. It is important to note that due to unexpected wind events, a single day was removed from one of the measuring heads.

Table 1.2. Chlorophyll fluorescence parameters, collected with the MONI-PAM fluorometer, their descriptions, and equations.

Parameter	Description
F_m	Maximum fluorescence after saturation pulse from dark adapted leaf
F_m'	Maximum fluorescence under light adapted conditions
F_s	Steady-state fluorescence under ambient light conditions
F_o	Minimal fluorescence from dark adapted leaf
$\frac{F_v}{F_m}$	Maximum quantum efficiency of PSII photochemistry; $\frac{F_m - F_o}{F_m}$ (Baker, 2008)
F_o'	Minimum fluorescence under light adapted conditions
PQ	Photochemical quenching; $\frac{F_m}{F_s} - \frac{F_m}{F_m`}$ (Porcar-Castell et al., 2014)
NPQ	Non-photochemical quenching ; $\frac{F_m - F_m`}{F_m`}$ (Porcar-Castell et al., 2014)

1.3.3.2 *Field hyperspectral spectroradiometer*

Leaf reflectance was measured at night using the same spectroradiometer as well as an attachment leaf clip (HR-1024i and LC-RP Pro, Spectra Vista Corporation, Poughkeepsie, New York, USA). The sampling frequency (# of days), and timing (waiting 15 minutes after light activation) of measurements remained the same as the canopy-level methodology (Table 1.1). Leaf sampling occurred immediately after the canopy-level spectral measurements, at night during the blue LED exposure time. To obtain a complete picture of what was happening

throughout the canopy, a series of 12 scans were taken: four random leaves in the top, followed by four in the middle, and finally four in the bottom third of the shrub. A white panel calibration, taken on Spectralon disks that are built into the leaf clip, was taken before each "section" of the shrub.

NDVI and PRI were computed for each leaf (n =12). Data were summarized to get the daily plant mean and standard deviation for each index. The following equations were used to calculated NDVI and PRI, where R represents reflectance in the respective waveband in the subscript:

$$NDVI = \frac{R_{800} - R_{680}}{R_{800} + R_{680}}$$

$$PRI = \frac{R_{531} - R_{570}}{R_{531} + R_{570}}$$

1.3.3.3 *Porometer/Fluorometer*

We used a LI-600 porometer to monitor stomatal conductance (g_{sw}) (LICOR Biosciences, Lincoln, Nebraska, USA). Default settings and auto-stabilization were used when taking measurements. Measurements were taken for 22 of the 25 days throughout the experiment (Table 1.1) and all samples took place within +/- 1 hour of solar noon. The sampling structure mimicked that of the leaf-level field spectrometer measurements, where a series of 12 scans were taken: four random leaves in the top, followed by four in the middle, and finally four in the bottom third of the shrub. A daily plant average, across all 12 leaves, was then calculated.

1.3.4 Data Analysis

Data handling, processing, and statistical analysis was conducted using R programming language (R Development Core Team, 2022). Linear regressions were run to compare the $LEDIF_{photodiode}$ setup performed against more traditionally acquired fluorescence and photosynthetic performance metrics. All analysis used daily means for comparisons across multiple instrument types.

1.4 Results

A typical drought response was observed across all parameters during the 30-day experiment (Fig. 1.3). There was a noticeable 1–2-day lag in response to the start of drought and return of normal watering conditions. At the canopy-level, both LED fluorescence metrics, $LEDIF_{photodiode}$ and $LEDIF_{hyperspectral,}$ decreased markedly when drought was induced (Fig. 1.3a-b). At the leaf-level, non-photochemical quenching (NPQ) increased whereas stomatal conductance (g_{sw}), $F_v/F_{m,}$ photochemical quenching (PQ), and F_o` decreased (Fig. 1.3c-g). In the short post-drought period, most metrics started to return to their baseline values as established in the pre-drought period. Notably, stomatal conductance (g_{sw}) never returned to "pre-drought" values. Leaf-level NDVI had little to no change over the entire duration of the experiment and never dropped below 0.8 (Fig. 1.3h). On the other hand, leaf-level PRI had a clear response to drought, mimicking the trends found in other leaf-level metrics. There was a dramatic decline in PRI ~1 day after the watering was ceased and a slight increase ~1 day after watering was reinitiated (Fig. 1.3i).

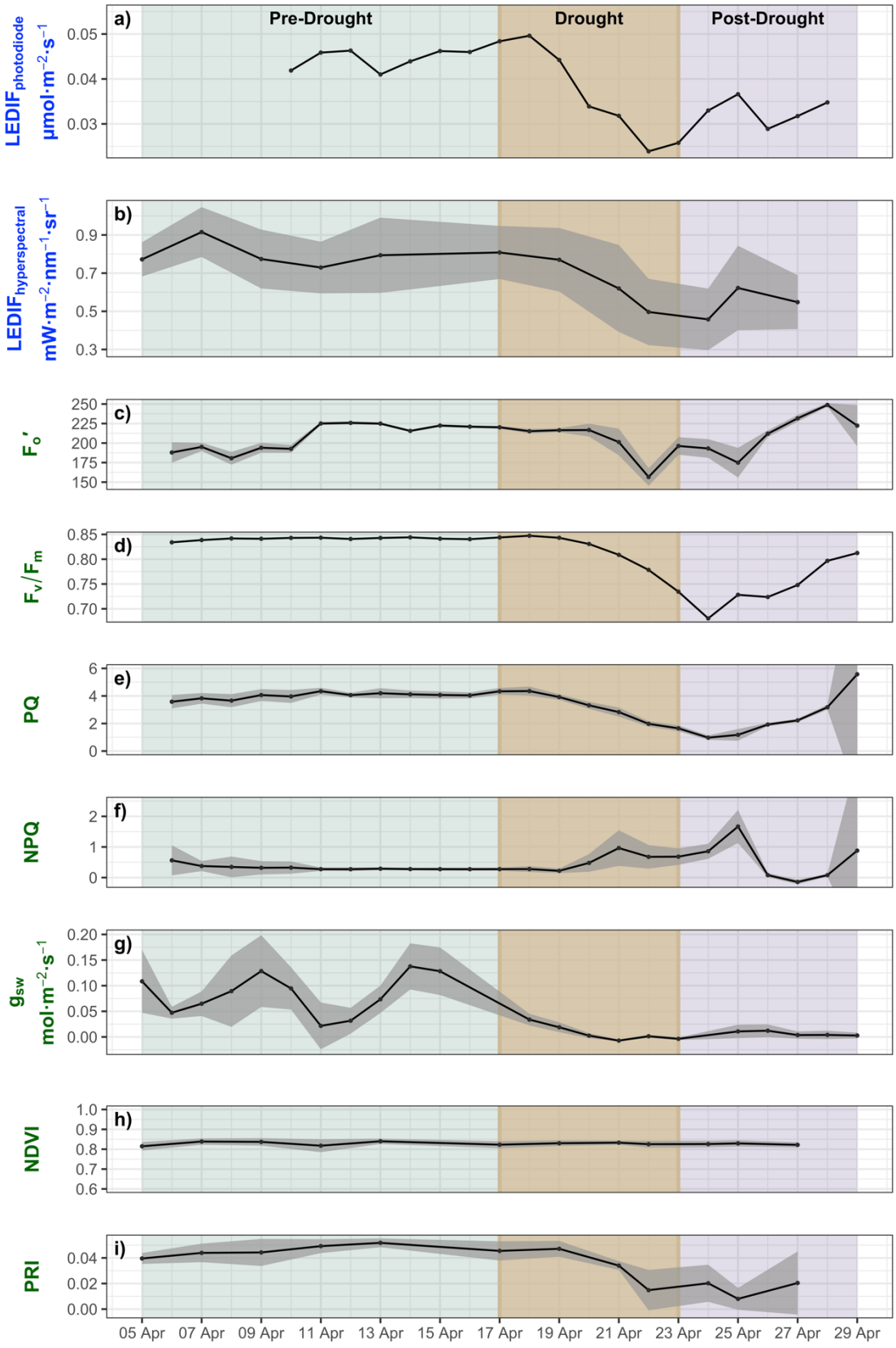
a)
Pre-Drought
Drought
Post-Drought
LEDIF photodiode
µmol·m⁻²·s⁻¹
0.05
0.04
0.03
b)
LEDIF hyperspectral
mW·m⁻²·nm⁻¹·sr⁻¹
0.9
0.7
0.5
0.3
c)
F₀'
250
225
200
175
150
d)
Fv/Fm
0.85
0.80
0.75
0.70
e)
PQ
6
4
2
0
f)
NPQ
2
1
0
g)
gsw
mol·m⁻²·s⁻¹
0.20
0.15
0.10
0.05
0.00
h)
NDVI
1.0
0.9
0.8
0.7
0.6
i)
PRI
0.04
0.02
0.00
05 Apr
07 Apr
09 Apr
11 Apr
13 Apr
15 Apr
17 Apr
19 Apr
21 Apr
23 Apr
25 Apr
27 Apr
29 Apr

Figure 1.3. Distinct periods throughout the study are indicated by distinct colors: green indicates pre-drought, brown indicates drought, and purple indicates post-drought. Blue text refers to canopy-level measurements, green text refers to leaf-level measurements. Note that not all measurements have the same y-axis scale. (a) shows the continuous low-cost broadband photodiode sensor LEDIF data, and (b) shows the hyperspectral spectroradiometer LEDIF data. (c)-(f) shows time-series of leaf-level parameters collected from the MONI-PAM instrument. (g) shows the stomatal conductance at leaf level from the LI-600 porometer. (h)-(i) shows time-series of calculated leaf-level vegetation indices (NDVI and PRI). For canopy-level: grey shaded regions indicate the standard deviation between the four scans taken on each sampling day. For leaf-level: grey shaded regions indicate the standard deviation between the twelve leaves scanned on each sampling day.

Linear regressions were performed to see how $LEDIF_{photodiode}$ values compared to the spectrometer measurements. At the canopy-level, $LEDIF_{hyperspectral}$ significantly correlated with $LEDIF_{photodiode}$ ($R^2=0.77, P < 0.01$) (Fig. 1.4a). Further, canopy-level $LEDIF_{photodiode}$ had a weaker relationship, with leaf-level steady-state fluorescence, (F_o`) measured with the MONI-PAM ($R^2 =0.22, P < 0.05$) (Fig. 1.4b). Other leaf-level PAM collected metrics also correlated with $LEDIF_{photodiode}$, with varying levels of significance and R^2 values (Fig. 1.4c-e). Stomatal conductance also correlates with steady-state canopy fluorescence — ($R^2=0.35, P < 0.05$)— (Fig. 1.4f). As for the vegetation indices, we did not find any significant trend between $LEDIF_{photodiode}$ and NDVI, but there was a positive trend ($R^2 =0.59, P < 0.05$) between PRI and $LEDIF_{photodiode}$ (Fig. 1.4g-h). Notably, most of the variance found in the regressions was found in the post-drought period data, except for g_{sw} where the variance was primarily found in the pre-drought period.

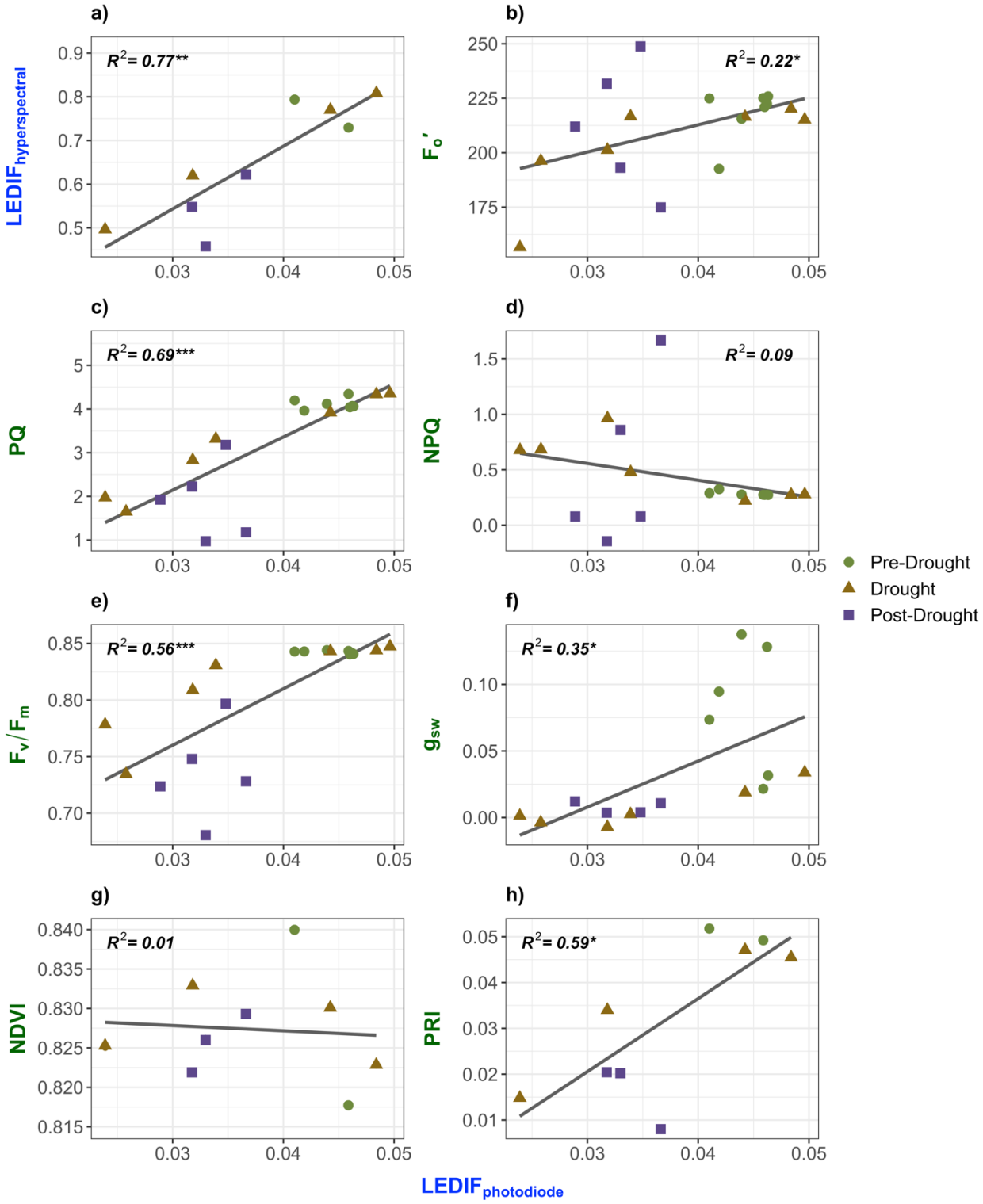
a)
b)
c)
d)
e)
f)
g)
h)
LEDIF hyperspectral
LEDIF photodiode
F o ’
PQ
NPQ
F v / F m
g sw
NDVI
PRI
R 2 = 0.77**
R 2 = 0.22*
R 2 = 0.69***
R 2 = 0.09
R 2 = 0.56***
R 2 = 0.35*
R 2 = 0.01
R 2 = 0.59*
Pre-Drought
Drought
Post-Drought

Figure 1.4. Correlations between canopy-level $LEDIF_{photodiode}$ and (a) $LEDIF_{hyperspectral}$, leaf-level (b) F_o', (c) PQ, (d) NPQ, (e) F_v/F_m, (f) stomatal conductance, (g) NDVI, & (h) PRI. Blue text refers to canopy-level measurements, green text refers to leaf-level measurements. Shapes refer to watering periods: green circle = pre-drought, brown triangle = drought, purple square = post-drought. The correlation and line fits are for all data points collected throughout the experiment; the stars represent p-values: * <0.05, ** <0.01, *** < 0.001.

1.5 Discussion

In this study, we were able to highlight changes in the drought response of canopy chlorophyll fluorescence in a broad-leaf evergreen shrub using a novel low-cost nighttime LED platform. Over the course of a month, we sought to meet two main objectives 1) track changes in canopy-level chlorophyll fluorescence with a new, nighttime, low-cost sensor during an imposed stress event and 2) test whether these changes are reflected at the canopy- and leaf-level. By incorporating the work of using LEDs to induce low-light steady-state chlorophyll fluorescence (Atherton et al. 2019) and dovetailing the inexpensive broadband photodiode sensors into our novel platform, we successfully built a setup that competed with more traditional, expensive setups to chlorophyll fluorescence remote sensing devices at both the leaf- and canopy-level.

1.5.1 Physiological Responses

Stomatal conductance, g_{sw}, which can be related to plant stress and water status (Buckley 2019) was measured throughout the experiment (Table 1.1). During the drought, we saw stomatal

conductance quickly decrease (Fig. 1.3g), signaling a closure of the stomata. Stomatal closure is a protective reaction of the plant in order to stop water loss (Buckley 2019). However, when the stomata close, the tradeoff is that there is also a cessation of incoming carbon (leaf gas exchange stops) and therefore a suspension photosynthesis (Ball, Woodrow, and Berry 1987). Although changes in the stomata and changes in photochemistry are not always necessarily coordinated (Marrs et al. 2020), we did find evidence of some coordination in our data, where g_{sw} was declining prior to PQ or NPQ decreasing and increasing, respectively (Fig 1.3g, e-f). This suggests that the stomata were responding quicker than the photochemical reactions, which has been observed at both the leaf- and canopy-level (Flexas et al. 2002; Marrs et al. 2020; Magney et al. 2020). Markedly, even after the drought ended, the stomatal activity did not recover to pre-drought values. In a vineyard drought experiment, Tombesi et al. (2015) similarly found that even after resuming watering post-drought, that the stomata in the grape leaves did not reopen. The fact that stomatal conductance did not trend toward recovery, is notable in comparison to all other parameters measured, which increased post-drought (Fig. 1.3). Additionally, in a drought stress experiment of kidney bean plants where the drought lasted 7+ days, Miyashita et al. (2005) also found that stomatal conductance was unable to fully recover post-drought but where photochemistry recovered more than 75% of its pre-drought levels (Miyashita et al., 2005). Furthermore, after a prolonged drought period, stomatal conductance was the only parameter, when regressed against $LEDIF_{photodiode}$, where most of the variance was held in the pre-drought data versus the post-drought data (Fig. 1.4f).

With reduced leaf-gas exchange, as suggested from our stomatal conductance measurements, we consequently saw a decrease in photosynthetic activity and altered energy balance, as shown

through our PAM parameters (Fig. 1.3c-f). As we know, there are three competing pathways in which absorbed photons can dissipate (Baker 2008). One way that plants cope with drought stress is by modulating their NPQ and PQ pathways. An increase in NPQ, as seen in our experiment, is a protective process in which excess light energy is dissipated as heat, which can also protect photosystem II from photo-oxidative damage (Baker 2008). Concurrently, PQ would be expected to decrease due to the lack of internal CO_2 and overall saturation of photosynthesis by light causing the subsequent reduction in active PSII reaction centers (Maxwell and Johnson 2000; Baker 2008). As expected, during the drought, we saw an increase in non-photochemical quenching, the subsequent decrease in photochemical quenching, as well as a decrease in Fv/Fm and Fo' (Fig. 1.3f-c, respectively). Additionally, our values of Fv/Fm— a sensitive indicator of plant photosynthetic performance (Maxwell and Johnson 2000)— decreased dramatically during the drought, which also tells us that there was a uptick in the efficiency of NPQ (Maxwell and Johnson 2000), further detailing the physiological stress that the plant was experiencing.

Further investigation led us into using remotely sensed proxies of light absorption and photoprotective pigments (chlorophylls and carotenoids/xanthophylls) during our induced drought. PRI provides us insight into photoprotective pigments— carotenoids that dynamically convert to expel excess absorbed energy when the plant is under stress or photosynthesis is saturated, and can therefore provide us a proxy of photosynthetic efficiency (Gamon et al. 1992; Demmig-Adams and Adams 1996; Gamon et al. 1997). During the drought period, we observed a reduction in PRI that directly mimicked the physiological parameters that were directly measuring the photosynthetic efficiency and photochemical quenching (Fig 1.3i). Although Gamon et al. (1992) found that PRI did not perform as well in water-stressed sunflowers at the

canopy-level, our leaf-level PRI data did provide insight into photosynthetic activity compared to PAM parameters and spectral canopy measurements. When PRI values were regressed against $LEDIF_{photodiode}$, we saw a relatively strong correlation, $R^2= 0.59, P<0.05$ (Fig. 1.4h), with a sharp decrease in the drought period and inklings of recovery in the post-drought period, as would be expected (Magney et al. 2016; Wong et al. 2022). We also investigated the NDVI, which provides us insight into the "greenness" of the plant and its chlorophyll content. NDVI did not prove insightful in detecting plant stress during the week-long imposed drought as there was little to no change in NDVI throughout the experiment (Fig. 1.3h), there was no visible change in greenness throughout the experiment. This makes sense given the short duration of the experiment – there was likely no change in leaf structure or chlorophyll concentration, making NDVI invariant.

When comparing the photodiode and hyperspectral LEDIF retrieval methods, our results demonstrated similar performance (Fig. 1.3 and 1.4; $R^2=0.77, P < 0.01$). This shows promise for a low-cost method to track temporal changes in canopy fluorescence emission (Fig. 1.3a-b; Fig. 1.4a). Not only this, but $LEDIF_{photodiode}$ tracked similar patterns in drought response of photosynthetic status indicated by PAM fluorescence measurements (Fig. 1.4). In particular, $LEDIF_{photodiode}$ correlated well with Fv/Fm ($R^2=0.59, P < 0.001$) indicating that we were able to capture changes in photosynthetic capacity and fluctuations of NPQ. Furthermore, $LEDIF_{photodiode}$ also correlated with PQ ($R^2=0.69, P < 0.001$) indicating that we were also able to track the leaf-level capacity of PSII at the canopy-level. With this, $LEDIF_{photodiode}$ indeed seems to be a meaningful indicator of photosynthetic status, and thus, overall plant "health".

1.5.2 Considerations and Conclusions

While the results of this experiment demonstrate the potential for using nighttime $LEDIF_{photodiode}$ measurements to track canopy-level chlorophyll fluorescence in a cost-effective way, some limitations should be considered. Although we were able to detect a fluorescence emission (Fig. 1.2), instigated by the blue LEDs, the signal that was recorded was relatively small (Fig. 1.2a). This may limit its effectiveness in the method being implemented in larger canopies or if the platform is placed higher above the canopy. Future studies may need to use stronger (greater than 15W) LEDs to overcome the weak signal. However, we caution that too strong of an LED may also lead to stomatal opening; ideally, increasing the signal to noise ratio while not inducing a photosynthetic response would be preferred. In addition, further research is needed to determine the effectiveness of this method in uncontrolled settings, such as croplands or forests in-situ, and at distances greater than 0.5 m from the top of the canopy. In a positive light, this methodology may serve as a way to validate SIF-yield data collected from tower-level measurements and species-specific responses within the field of view of a tower.

Strong stress may also induce structural changes in the canopy (e.g., wilting). It is challenging to separate structural changes from physiological changes when using remote sensing methods to measure photosynthesis or, in our case, chlorophyll fluorescence. Even though a structural change was not observed in our study, understanding how to disentangle or account for structural changes when measuring canopy fluorescence could potentially improve the interpretation and generalizability of the results. One approach may be to normalize the far-red LEDIF by reflected

light in the LED light region (e.g., blue light). This could help account for variation in canopy structure to enhance the SIF signal (Magney et al., 2019; Pierrat et al. 2021).

In summary, the successful implementation of our labor-reducing, low-cost canopy-based, nighttime LEDIF system in this study demonstrates its potential for use in future research and highlights the need for continued exploration of the capabilities and limitations of such remote sensing tools. The development of new and innovative tools to measure plant stress is crucial for advancing our understanding of plant physiological responses to environmental stressors, the connections between the physiological mechanisms linking chlorophyll fluorescence and photosynthesis at multiple scales, and for the development of effective strategies for mitigating the impacts of climate change in our natural ecosystems.

1.6 References

Allen CD, Macalady AK, Chenchouni H, *et al.* 2010. A global overview of drought and heat-induced tree mortality reveals emerging climate change risks for forests. *Forest Ecology and Management* **259**: 660–684.

Atherton J, Liu W, Porcar-Castell A. **2019**. Remote Sensing of Environment Nocturnal Light Emitting Diode Induced Fluorescence (LEDIF): A new technique to measure the chlorophyll a fluorescence emission spectral distribution of plant canopies in situ. *Remote Sensing of Environment* **231**: 111137.

Baker NR. **2008**. Chlorophyll fluorescence: A probe of photosynthesis in vivo. *Annual Review of Plant Biology***59**: 89–113.

Baker, Neil R., Oxborough, Kevin (2004). "Chlorophyll Fluorescence as a Probe of Photosynthetic Productivity". *Chlorophyll a Fluorescence*. Advances in Photosynthesis and Respiration. **19**. pp. 65–82**.**

Baldocchi DD. 2003. Assessing the eddy covariance technique for evaluating carbon dioxide exchange rates of ecosystems: Past, present and future. *Global Change Biology* **9:** 479–492.

Baret F, Guyot G. **1991**. Potentials and limits of vegetation indices for LAI and APAR assessment. *Remote Sensing of Environment* **35**: 161–173.

Ball JT, Woodrow IE, Berry JA. 1987. A model predicting stomatal conductance and its contribution to the control of photosynthesis under different environmental conditions. In: Biggens J, eds. *Progress in photosynthesis research*. Leiden, the Netherlands: Martinus Nijhoff, 221–224.

Beer C, Reichstein M, Tomelleri E, *et al.* 2010. Terrestrial gross carbon dioxide uptake: Global distribution and covariation with climate. *Science* **329**: 834–838.

Buckley TN. **2019**. How do stomata respond to water status? *New Phytologist* **224**: 21–36.

Chiang F, Mazdiyasni O, AghaKouchak A. **2021**. Evidence of anthropogenic impacts on global drought frequency, duration, and intensity. *Nature Communications* **12**: 1–10.

Choat B, Jansen S, Brodribb TJ, *et al.* 2012. Global convergence in the vulnerability of forests to drought. *Nature* **491**: 752–755.

Demmig-Adams B, Adams WW. **1996**. The role of xanthophyll cycle carotenoids in the protection of photosynthesis. *Trends in Plant Science* **1**: 21–26.

Fichot R, Brignolas F, Cochard H, Ceulemans R. **2015**. Vulnerability to drought-induced cavitation in poplars: Synthesis and future opportunities. *Plant Cell and Environment* **38**: 1233–1251.

Flexas J, Escalona JM, Evain S, *et al.* 2002. Steady-state chlorophyll fluorescence (Fs) measurements as a tool to follow variations of net CO2 assimilation and stomatal conductance during water-stress in C3 plants. *European Space Agency, (Special Publication) ESA SP*: 26–29.

Flexas JA, Bota J, Escalona JM, Sampol B, Medrano H. **2002**. Effects of drought on photosynthesis in grapevines under field conditions: an evaluation of stomatal and mesophyll limitations. *Functional Plant Biology* **29**: 461–471.

Frankenberg C, Fisher JB, Worden J, *et al.* 2011. New global observations of the terrestrial carbon cycle from GOSAT: Patterns of plant fluorescence with gross primary productivity. *Geophysical Research Letters* **38**: 1–6.

Gamon JA, Serrano L, Surfus JS. **1997**. The photochemical reflectance index: An optical indicator of photosynthetic radiation use efficiency across species, functional types, and nutrient levels. *Oecologia* **112**: 492–501.

Gamon JA, Penuelas J, Field CB. **1992**. A Narrow-Waveband Spectral Index That Tracks Diurnal Changes in Photosynthetic Efficiency*. *Remote Sensing of Environment* **41**: 35–44.

Garbulsky MF, Peñuelas J, Gamon J, Inoue Y, Filella I. **2011**. The photochemical reflectance index (PRI) and the remote sensing of leaf, canopy and ecosystem radiation use efficiencies. A review and meta-analysis. *Remote Sensing of Environment* **115**: 281–297.

Glenn EP, Huete AR, Nagler PL, Nelson SG. **2008**. Relationship between remotely-sensed vegetation indices, canopy attributes and plant physiological processes: What vegetation indices can and cannot tell us about the landscape. *Sensors* **8**: 2136–2160.

Grossmann K, Frankenberg C, Magney TS, Hurlock SC, Seibt U, Stutz J. **2018**. PhotoSpec: A new instrument to measure spatially distributed red and far-red Solar-Induced Chlorophyll Fluorescence. *Remote Sensing of Environment* **216**: 311–327.

Helm LT, Shi H, Manuel LT, Yang X. **2020**. Solar-induced chlorophyll fluorescence and short-term photosynthetic response to drought. *Ecological Applications* **30**: 1–12.

Huang X, Xiao J, Ma M. **2019**. Evaluating the performance of satellite-derived vegetation indices for estimating gross primary productivity using FLUXNET observations across the globe. *Remote Sensing* **11**.

Huete AR, Liu HQ, van Leeuwen WJD. **1997**. Use of vegetation indices in forested regions: Issues of linearity and saturation. *International Geoscience and Remote Sensing Symposium (IGARSS)* **4**: 1966–1968.

Joiner J, Yoshida Y, Vasilkov AP, Yoshida Y, Corp LA, Middleton EM. **2011**. First observations of global and seasonal terrestrial chlorophyll fluorescence from space. *Biogeosciences* **8**: 637–651.

Kautsky H, Hirsch A. **1931**. Neue Versuche zur Kohlensäureassimilation. *Die Naturwissenschaften* **19**: 964.

Kimm H, Guan K, Burroughs CH, *et al.* 2021. Quantifying high-temperature stress on soybean canopy photosynthesis: The unique role of sun-induced chlorophyll fluorescence. *Global Change Biology* **27**: 2403–2415.

Lin S, Li J, Liu Q, Li L, Zhao J, Yu W. **2019**. Evaluating the effectiveness of using vegetation indices based on red-edge reflectance from Sentinel-2 to estimate gross primary productivity. *Remote Sensing* **11**.

Litchenthaler HK. **1992**. The Kautsky effect: 60 years of chlorophyll fluorescence induction kinetics. *Photosynthetica* **27**: 45–55.

Magney TS, Bowling DR, Logan BA, *et al.* 2019. Mechanistic evidence for tracking the seasonality of photosynthesis with solar-induced fluorescence. *Proceedings of the National Academy of Sciences of the United States of America* **116**: 11640–11645.

Magney TS, Frankenberg C, Fisher JB, *et al.* 2017. Connecting active to passive fluorescence with photosynthesis: a method for evaluating remote sensing measurements of Chl fluorescence. *New Phytologist***215**: 1594–1608.

Magney TS, Vierling LA, Eitel JUH, Huggins DR, Garrity SR. **2016**. Response of high frequency Photochemical Reflectance Index (PRI) measurements to environmental conditions in wheat. *Remote Sensing of Environment* **173**: 84–97.

Marrs JK, Reblin JS, Logan BA, *et al.* 2020. Solar-Induced Fluorescence Does Not Track Photosynthetic Carbon Assimilation Following Induced Stomatal Closure. *Geophysical Research Letters* **47**: 1–11.

Maxwell K, Johnson GN. **2000**. Chlorophyll fluorescence—a practical guide. *Journal of Experimental Botany* **51**: 659–668.

Meroni M, Rossini M, Guanter L, *et al.* 2009. Remote sensing of solar-induced chlorophyll fluorescence: Review of methods and applications. *Remote Sensing of Environment* **113**: 2037–2051.

Miyashita K, Tanakamaru S, Maitani T, Kimura K. **2005**. Recovery responses of photosynthesis, transpiration, and stomatal conductance in kidney bean following drought stress. *Environmental and Experimental Botany* **53**: 205–214.

Mohammed GH, Colombo R, Middleton EM, *et al.* 2019. Remote sensing of solar-induced chlorophyll fluorescence (SIF) in vegetation: 50 years of progress. *Remote Sensing of Environment* **231**: 111177.

Murchie EH, Lawson T. **2013**. Chlorophyll fluorescence analysis: A guide to good practice and understanding some new applications. *Journal of Experimental Botany* **64**: 3983–3998.

Peng Y, Gitelson AA. **2011**. Application of chlorophyll-related vegetation indices for remote estimation of maize productivity. *Agricultural and Forest Meteorology* **151**: 1267–1276.

Pierrat Z, Nehemy MF, Roy A, *et al.* 2021. Tower-Based Remote Sensing Reveals Mechanisms Behind a Two-phased Spring Transition in a Mixed-Species Boreal Forest. *Journal of Geophysical Research: Biogeosciences* **126**: 1–20.

Pierrat Z, Magney T, Parazoo NC, *et al.* 2022. Diurnal and Seasonal Dynamics of Solar-Induced Chlorophyll Fluorescence, Vegetation Indices, and Gross Primary Productivity in the Boreal Forest. *Journal of Geophysical Research: Biogeosciences* **127**.

Porcar-Castell A, Malenovský Z, Magney T, *et al.* 2021. Chlorophyll a fluorescence illuminates a path connecting plant molecular biology to Earth-system science. *Nature Plants* **7**: 998–1009.

Porcar-Castell A, Tyystjärvi E, Atherton J, *et al.* 2014. Linking chlorophyll a fluorescence to photosynthesis for remote sensing applications: Mechanisms and challenges. *Journal of Experimental Botany* **65**: 4065–4095.

R Development Core Team. 2020. R: A Language and Environment for Statistical Computing. http://www.r-project.org/.

Romero JM, Cordon GB, Lagorio MG. **2018**. Modeling re-absorption of fluorescence from the leaf to the canopy level. *Remote Sensing of Environment* **204**: 138–146.

Romero JM, Otero A, Lagorio MG, Berger AG, Cordon GB. **2021**. Canopy active fluorescence spectrum tracks ANPP changes upon irrigation treatments in soybean crop. *Remote Sensing of Environment* **263**.

Rousta I, Olafsson H, Moniruzzaman M, *et al.* 2020. Impacts of drought on vegetation assessed by vegetation indices and meteorological factors in Afghanistan. *Remote Sensing* **12**.

Ryu Y, Berry JA, Baldocchi DD. **2019**. What is global photosynthesis? History, uncertainties and opportunities. *Remote Sensing of Environment* **223**: 95–114.

Sarlikioti V, Driever SM, Marcelis LFM. **2010**. Photochemical reflectance index as a mean of monitoring early water stress. *Annals of Applied Biology* **157**: 81–89.

Sun Y, Frankenberg C, Wood JD, *et al.* 2017. OCO-2 advances photosynthesis observation from space via solar-induced chlorophyll fluorescence. *Science* **358**.

Sun Y, Frankenberg C, Jung M, *et al.* 2018. Overview of Solar-Induced chlorophyll Fluorescence (SIF) from the Orbiting Carbon Observatory-2: Retrieval, cross-mission comparison, and global monitoring for GPP. *Remote Sensing of Environment* **209**: 808–823.

Sun Y, Ren H, Zhang T, Zhang C, Qin Q. **2018**. Crop Leaf Area Index Retrieval Based on Inverted Difference Vegetation Index and NDVI. *IEEE Geoscience and Remote Sensing Letters* **15**: 1662–1666.

Sun Z, Wang X, Zhang X, *et al.* 2019. Evaluating and comparing remote sensing terrestrial GPP models for their response to climate variability and CO 2 trends. *Science of the Total Environment* **668**: 696–713.

Tucker CJ. **1979**. Red and photographic infrared linear combinations for monitoring vegetation. *Remote Sensing of Environment* **8**: 127–150.

Turner DP, Ritts WD, Cohen WB, *et al.* 2006. Evaluation of MODIS NPP and GPP products across multiple biomes. *Remote Sensing of Environment* **102**: 282–292.

Verma M, Schimel D, Evans B, *et al.* 2017. Effect of environmental conditions on the relationship between solar-induced fluorescence and gross primary productivity at an OzFlux grassland site. *Journal of Geophysical Research: Biogeosciences* **122**: 716–733.

Vilagrosa A, Bellot J, Vallejo VR, Gil-Pelegrín E. **2003**. Cavitation, stomatal conductance, and leaf dieback in seedlings of two co-occurring Mediterranean shrubs during an intense drought. *Journal of Experimental Botany* **54**: 2015–2024.

Wagle P, Xiao X, Torn MS, *et al.* 2014. Sensitivity of vegetation indices and gross primary production of tallgrass prairie to severe drought. *Remote Sensing of Environment* **152**: 1–14.

Wong CYS, Bambach NE, Alsina MM, *et al.* 2022. Detecting short-term stress and recovery events in a vineyard using tower-based remote sensing of photochemical reflectance index (PRI). *Irrigation Science* **40**: 683–696.

Wu J, Serbin SP, Ely KS, *et al.* 2019. The response of stomatal conductance to seasonal drought in tropical forests. *Global Change Biology* **26**: 823–839.

Xiao J, Chevallier F, Gomez C, *et al.* 2019. Remote sensing of the terrestrial carbon cycle: A review of advances over 50 years. *Remote Sensing of Environment* **233**: 111383.

Xue J, Su B. **2017**. Significant remote sensing vegetation indices: A review of developments and applications. *Journal of Sensors* **2017**.

Yang X, Shi H, Stovall A, *et al.* 2018. FluoSpec 2—an automated field spectroscopy system to monitor canopy solar-induced fluorescence. *Sensors (Switzerland)* **18**.

Yang X, Tang J, Mustard JF, *et al.* 2015. Solar-induced chlorophyll fluorescence that correlates with canopy photosynthesis on diurnal and seasonal scales in a temperate deciduous forest. *Geophysical Research Letters* **42**: 2977–2987.

Zhang C, Filella I, Liu D, *et al.* 2017. Photochemical Reflectance Index (PRI) for detecting responses of diurnal and seasonal photosynthetic activity to experimental drought and warming in a Mediterranean shrubland. *Remote Sensing* **9**: 1–21.

Zhang Y, Ye A. **2021**. Would the obtainable gross primary productivity (GPP) products stand up? A critical assessment of 45 global GPP products. *Science of the Total Environment* **783**: 146965.

2 Hyperspectral Reflectance-Based Prediction of Pigment Concentrations in *Pinus palustris* (Longleaf Pine) Using Partial Least Squares Regression Modeling

Logan E.G. Brissette, Chris Y.S. Wong, Sara Nelson, Barry Logan, and Troy S. Magney

2.1 Abstract

Photosynthesis is a critical process by which plants convert sunlight into chemical energy, relying on a variety of pigments to regulate light absorption, energy transfer and photoprotection. This study aims to predict eight chlorophyll and carotenoid pigments and their pools in *Pinus palustris* using leaf-level hyperspectral reflectance measurements and partial least squares regression (PLSR) modeling. This study took place in north-central Florida, at the Ordway Swisher Biological Station (OSBS), and more specifically, the National Ecological Observation Network (NEON) flux tower site within it. The research site is dominated by mature Longleaf Pines and low-lying perennial grasses. From six Longleaf Pine trees, branches were harvested, and needles were either 1) immediately stored for later pigment extraction and 2) made into needle mats to retrieve reflectance measurements with our hyperspectral spectroradiometer's leaf clip. Needle mats were assembled by laying individual needles flat and continuously side by side until they were approximately 5-6 cm wide, and were held together by two pieces of tape, arranged at the top and bottom of the needles. Using a PLSR modeling approach, our prediction task for each PLSR model was to predict the average pigment content of a tree, using a hyperspectral reflectance measurement of a single needle mat (for each pigment/pool) per

tree. Our PLSR models successfully predicted the concentrations with R^2 values > 50% for eight of the ten pigments/pools, supporting the potential of hyperspectral remote sensing to estimate pigment concentrations with relatively high accuracy. We were able to best predict lutein and neoxanthin, as well as chlorophyll *b* and *a* ($R^2 = 0.91$, $RMSE = 0.01$; $R^2 = 0.77$, $RMSE = 0.0$; $R^2 = 0.68$, $RMSE = 0.02$; $R^2 = 0.65$, $RMSE = 0.05$, respectively).Variable importance in projection scores revealed the green and red-edge spectral regions as consistently important for all pigments, further highlighting the importance of chlorophylls and carotenoids in their roles in responding to seasonal environmental changes via photoprotection and energy transfer efficiency. These findings demonstrate the value of leaf-level remote sensing in understanding the physiological status of evergreen species and their underlying pigments, as well as the potential of hyperspectral remote sensing to advance our knowledge of plant physiology at larger scales.

2.2 Introduction

Photosynthesis, the process by which plants convert sunlight into chemical energy, relies on a myriad of specific pigments that not only capture light but also play crucial roles in regulating the efficiency of energy transfer and photoprotection (Demmig-Adams and Adams, 1996). In particular, chlorophyll and carotenoid pigments (such as violaxanthin, neoxanthin, antheraxanthin, lutein, chlorophyll *a*, chlorophyll *b*, alpha-carotene, and beta-carotene) are essential for optimal leaf function. For example, chlorophylls, particularly chlorophyll *a* and *b*, are primarily responsible for light absorption and energy transfer, as they constitute the backbone of the photosynthetic machinery (Palta 1990; Melkozernov and Blankenship 2006). Carotenoids,

including alpha-carotene, beta-carotene, lutein, and neoxanthin, serve various protective functions, such as preventing photooxidative damage, scavenging reactive oxygen species, and quenching harmful triplet-state chlorophylls (Dall'Osto et al. 2007; Cazonelli 2011, Jahns and Holzwarth 2012; Giossi et al. 2020). Xanthophyll cycle pigments —which can include violaxanthin, antheraxanthin, zeaxanthin— and lutein help to modulate photosynthetic processes by capturing specific wavelengths of light, dissipating excess energy, and maintaining the structural integrity of the photosynthetic machinery (Demmig-Adams and Adams 1996; Lu et al. 2001; Demmig-Adams and Adams 2006; Jahns and Holzwarth 2012). Understanding the importance of each group of pigments in photosynthetic regulation is essential for advancing our knowledge of photosynthesis, carbon uptake, and plant ecology on the whole.

Remote sensing of pigments at the leaf-level has significantly advanced our understanding of the roles and interactions of various pigments in photosynthesis and their responses to environmental changes (Gamon et al. 1990, 1992; Gitelson and Merzlyak 1996; Xue and Yang 2009). Leaf-level remote sensing techniques often use spectroscopy, which measures the reflectance, transmittance, and absorbance properties of leaves across a wide range of wavelengths. Examining spectral connections to plant pigments provides insights into the concentration and dynamics of pigments, such as chlorophylls and carotenoids, and their relationship to photosynthesis and plant health (Blackburn 2007; Ustin et al. 2009). This approach has led to the development of vegetation indices, allowing deeper insights into plant physiological status (Tucker 1979; Gamon et al., 1990, 1992, 2016, Sims and Gamon 2002; Badgley et al. 2017). As an example, Gamon et al. (1992) developed the Photochemical Reflectance Index (PRI), a narrow-waveband spectral index, which tracks diurnal changes in photosynthetic efficiency by

capturing variations in the xanthophyll pigments involved in the xanthophyll cycle. This index has been extensively used to study the dynamic regulation of photosynthetic processes at the leaf level, providing insights into the role of pigments in photoprotection and energy dissipation (Garbulksy et al. 2011; Magney et al. 2016). Furthermore, other leaf-level studies, such as Gitelson, Gritz, and Merzlyak (2003), have demonstrated the use of remote sensing to estimate chlorophyll content, an essential parameter for understanding photosynthetic capacity and plant productivity. Moreover, leaf-level remote sensing has proven valuable in understanding plant responses to various environmental stressors, such as drought, temperature extremes, and nutrient limitations, by observing changes in pigment concentrations and photosynthetic activity (Xue and Yang 2009; Magney et al. 2016; Helm et al. 2020, Wong et al. 2020).

Partial least squares regression (PLSR) has emerged as a powerful multivariate modeling approach for predicting leaf-traits, including pigment concentrations, based on remotely sensed spectral data (Serbin et al. 2012, 2014; Steidle Neto et al. 2016; Burnett et al. 2021, Mahajan et al. 2021). One of the key advantages of PLSR is its ability to handle collinear and noisy data (Wold et al. 2001), which are common features in the high-dimensional reflectance spectra obtained from remote sensing measurements (Serbin et al. 2012, 2014). PLSR deals with collinearity and high dimensionality by reducing the large predictor matrix— that would come from hyperspectral reflectance data, identifying the most relevant latent components that encompass and explain the most significant variation in the data, and overall providing higher parameter stability than classical regression (Geladi and Kowalski 1986, Wolter et al. 2008; Serbin et al. 2014).

The PLSR modeling approach is particularly useful for predicting leaf traits because it incorporates information from the entire spectrum, rather than relying on single or narrow bands, as is often the case with traditional vegetation indices. This comprehensive utilization of spectral information allows PLSR models to capture subtle variations in leaf traits that might be overlooked by more simplistic approaches. Furthermore, by calculating variable importance in projection (VIP) scores, PLSR can be used to identify the most informative wavelengths for predicting leaf traits, providing insight into the relative importance of spectral bands in explaining the variation in the model inputs (He et al. 2015). This, in turn, enables us to gain further insights into the complex relationships between leaf-level remote sensing and plant physiology.

The development of robust predictive models for estimating pigment concentrations at the needle scale is vital for progressing our ability to monitor and understand plant physiology at larger scales, such as canopy, landscape, and regional levels (Blackburn 2006; Porcar-Castell et al. 2014, 2021; Schimel et al. 2019). This scaling-up process is of particular importance in the context of recent advancements in remote sensing technology, including new hyperspectral missions like the NASA Surface Biology and Geology (SBG) mission (Cawse-Nicholson et al. 2023) and the Airborne Visible/Infrared Imaging Spectrometer-Next Generation (AVIRIS-NG) airborne mission (Thompson et al., 2019). These missions offer fine-scale spectral resolution and large spatial coverage, enabling researchers to capture detailed information on pigment dynamics across diverse ecosystems and environmental gradients. By elucidating the roles of different pigment groups, their interactions, and the mechanisms by which they regulate photosynthetic

processes, we can enhance interpretability of remote sensing data and develop more effective methodologies for monitoring plant responses to environmental changes (Blackburn 2006).

Despite previous research predicting leaf traits through spectrometry, indices, and various modeling techniques (Serbin et al. 2012, 2014, Huang et al. 2015; Steidle Neto et al. 2016; Mahajan et al. 2021, Wong et al. 2023), predicting a whole suite of pigments' content through hyperspectral measurements for an evergreen species has yet to be thoroughly investigated at the leaf-level. Therefore, in this study we aim to use hyperspectral reflectance (400 nm to 2400 nm) measurements taken on needle mats to predict eight pigments and two pigment pools (violaxanthin, neoxanthin, antheraxanthin, lutein, chlorophyll *a*, chlorophyll *b*, α-carotene, β-carotene, V+A+Z, and chlorophyll *a* + chlorophyll *b*) in *Pinus palustris*, Longleaf Pine, by using a PLSR modeling approach.

2.3 Methods and materials

2.3.1 Field Site

Fieldwork took place in north-central Florida, at the Ordway Swisher Biological Station (OSBS) in Putnam County, about 20 miles east of Gainesville. The OSBS is managed and cared for by the University of Florida as a biological site and the National Ecological Observation Network (NEON) southeastern domain 03. The north central Floridian climate is characterized as humid subtropical, with mild winters, hot and humid summers, and most of the precipitation occurring in the months June through September. As a biological field station, OSBS is a patchwork of

vegetative plots at varying life stages and undergoing a variety of management treatments, but generally, OSBS dominated by hardwoods (turkey oak) and conifers (Longleaf Pine - *Pinus palustris* and Loblolly Pine- *Pinus taeda*).

Sampling occurred within the flux tower footprint of a site established by NEON in 2014. This research site is dominated by mature Longleaf Pines and low-lying perennial grasses. Six trees were chosen, flagged, and labeled (PIPA 1:6) within 50 meters of the tower and were repeatedly sampled over three visits in 2021-2022: June & October 2021 and January 2022.

2.3.2 Hyperspectral Measurements

Pine branches were harvested in the early morning, with the stem placed in water and re-cut, prior to being processed. From the harvested branches, individual needles were separated from the needle bunches. Following the methodology of the continuous needle mat configuration by Rajewicz et al. (2019) needles were laid flat and adjacent to each other, limiting the space between needles without overlapping them, to make a leaf mat that was capable of scanning with our field spectrometer leaf clip. The needles were held together by two pieces of tape, arranged at the top and bottom of the mat (Fig. 2.1). Healthy, mature needles were chosen randomly from their originating branch. A typical mat was 5 cm - 6 cm wide and 10 cm - 15 cm long between the two pieces of tape.

Once the mat was created, our hyperspectral spectroradiometer with a leaf clip assembly attachment was used to measure reflectance spectra from 400 nm to 2,400 nm (SVC HR-1024i,

LC-RP Pro, Spectra Vista Corporation, Poughkeepsie, New York, USA). The leaf clip assembly attachment had an internal, regulated light source, built-in Spectralon white calibration disks, and UB black disk (<5% reflectance) (LC-RP Pro, Spectra Vista Corporation, Poughkeepsie, New York, USA). The specifications on this spectroradiometer were a 25° FOV optic fiber and an integration time of 1s. We chose to use the low-lamp-light intensity setting (2.8 Watts) on the leaf-clip. White panel calibrations (taken on Spectralon disks that were built into the leaf clip), were taken between every individual mat (every five scans). Spectral regions were filtered out from 920 nm to 1,040 nm due to instrumental-specific hot pixels.

For every mat, five scans were taken across the mat, so that a different part of the leaf mat was incorporated each time (Fig. 2.1). The sampling structure was as follows: five trees were sampled per visit, each tree had one branch harvested per visit. Each branch had three mats made, where five scans of each mat were taken. Therefore, fifteen scans were taken of each tree per site visit. In total there were 255 samples taken, as one flagged tree was unlocatable during our June 2021 visit.

Figure 2.1: shows a constructed needle mat held together with tape. Illustrated circles represent the configuration of where scans would be taken with the leaf-clip.

2.3.3 Pigment collection

Needle pigment composition was measured to relate to spectral measurements. Simultaneous to the spectral measurements being collected, needles from the same branch were collected, wrapped in foil, and immediately flash-frozen in liquid nitrogen until they were transported back to the lab where they were held in a -80 ℃ freezer until they were extracted. Pigments were extracted in acetone and analyzed by HPLC as described in Bowling et al. (2018). Pigments

extracted included: violaxanthin, neoxanthin, antheraxanthin, lutein, zeaxanthin, chlorophyll *b*, chlorophyll *a*, alpha-carotene, and beta-carotene. Pools focused on for data analysis where chlorophyll *a* + chlorophyll *b*, and violaxanthin + antheraxanthin + zeaxanthin. Pigment information was summarized per tree and referenced back to the corresponding tree's spectral information. Needle pigment contents are expressed as moles per fresh mass (μmol per gram).

2.3.4 Data Analysis

Spectral and pigment data were analyzed using a partial least-squares regression (PLSR) modeling approach (Wold et al. 1984, 2001; Geladi and Kowalski 1986; Serbin et al. 2012, 2014) to predict leaf pigment pools from hyperspectral reflectance measurements. PLSR modeling is a robust method for applied ecological remote sensing research. (Smith et al., 2002; Wolter et al., 2008; Askari et al., 2019; Mahajan et al., 2021). Most importantly, though, PLSR provides ecologists the opportunity to turn a massive amount of remotely sensed data into interpretable results. In our case, in this study, it provides the opportunity to investigate the relationship between spectral bands and pigment/pools within leaves.

Data handling, processing, and statistical analysis was conducted using R open-source statistical environment (R Development Core Team, 2022), utilizing the PLS package (Mevik and Wehrens 2007). Initial pigment data handling and preparation for analysis was done in Microsoft Excel (Microsoft Corporation, 2021). The prediction task for the PLSR model was to predict the average pigment content of a tree, using a hyperspectral reflectance measurement of a single needle mat (for each of the 8 pigment types and 2 pigment pools) per tree. For each individual

needle mat there were five hyperspectral spectral measurements taken and three mats made per tree, giving us fifteen hyperspectral measurements total per tree. Each of these spectral measurements were related to their respective single averaged tree pigment value. We did not build separate models for individual visits to the site (June, October, and January) but individualized models were run for each of the 8 pigments and 2 pigment pools. For example, for a single pigment "lutein" there were seventeen trees sampled across our three field excursions. For each of the seventeen trees, there were fifteen hyperspectral measurements taken, giving us 255 samples. Our spectral-pigment data (n= 255) was split for model calibration (70%; n= 178), and validation (30%; n= 77), ensuring that the sets were representative of the full range of spectral values (Fig. 2). PLSR models were calibrated following the recommendations of Burnett et al. (2021); the optimal number of components included in each model was based on the firstMin method with a maximum number of components equaling 20. The predictive extent of the models was evaluated by the root mean square error (RMSE) and coefficient of determination (R^2) and variable importance in projection (VIP) (Wold et al. 2001, He et al. 2015; Burnett et al. 2021).

2.4 Results

The reflectance of the needle leaf mats varied only by 10-25% across the full spectrum, and was comparable for both the validation and calibration samples (Fig. 2.2). There was slightly less variation in the red-edge and NIR region in the validation dataset compared to the calibration

dataset (Fig. 2.2).

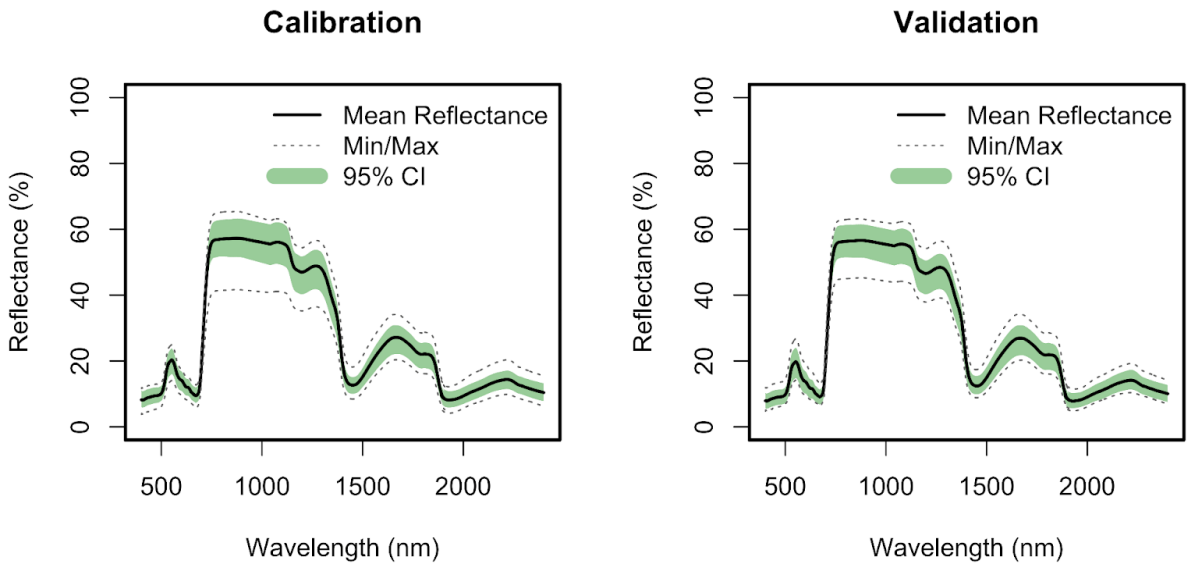

Figure 2.2. Shows the spectral reflectance: mean, minimum/maximum and 95% confidence interval (CI) from needle leaf mats. a) shows the spectral reflectance values for the calibration dataset, n = 178. b) shows the spectral reflectance values for the validation dataset, n = 77.

All eight individual pigments and two pigment pools were well-predicted by our hyperspectral reflectance informed PLSR models, with eight of the ten pigments reporting coefficient of determination values > 50% as well as RMSE values for eight pigments <0.02 (Fig. 2.3, Table 2.1). PLSR predictions using hyperspectral reflectance best predicted pigments lutein (Fig. 2.3g; $R^2 = 0.91$, $RMSE = 0.01$), followed by neoxanthin (Fig. 2.3h; $R^2 = 0.77$, $RMSE = 0.00$). The PLSR models for chlorophyll *b* (Fig. 2.3f), chlorophyll *a* (Fig. 2.3e), VAZ (Fig. 2.3i), Chl *a* + Chl *b* (Fig. 2.3d), α-carotene (Fig. 2.3a), and β-carotene (Fig. 2.3c) displayed moderate predictive performance with R^2 values between 0.58 and 0.68 while the PSLR models for Antheraxanthin and Violaxanthin showed the lowest coefficients of determination (Fig. 2.3b $R^2 = 0.43$; Fig. 2.3j $R^2 = 0.45$, respectively).

Table 2.1. Summary of results from the hyperspectral reflectance informed PLSR models (calibration and validation) predicting the eight pigments and two pigment pools. All values (calibration and validation) were found to be significant, with p-values that were all smaller than 10^{-12}.

		R^2		RMSE	
Pigment	Number of Components	Calibration	Validation	Calibration	Validation
α-carotene	12	0.53	0.60	0.01	0.01
Antheraxanthin	9	0.61	0.43	0.00	0.00
β-carotene	12	0.49	0.58	0.01	0.01
Chl a + Chl b	13	0.59	0.61	0.07	0.07
Chlorophyll a	14	0.65	0.66	0.05	0.05
Chlorophyll b	11	0.68	0.68	0.02	0.02
Lutein	11	0.87	0.91	0.01	0.01
Neoxanthin	11	0.73	0.77	0.00	0.00
VAZ	14	0.66	0.63	0.01	0.01
Violaxanthin	11	0.60	0.45	0.00	0.00

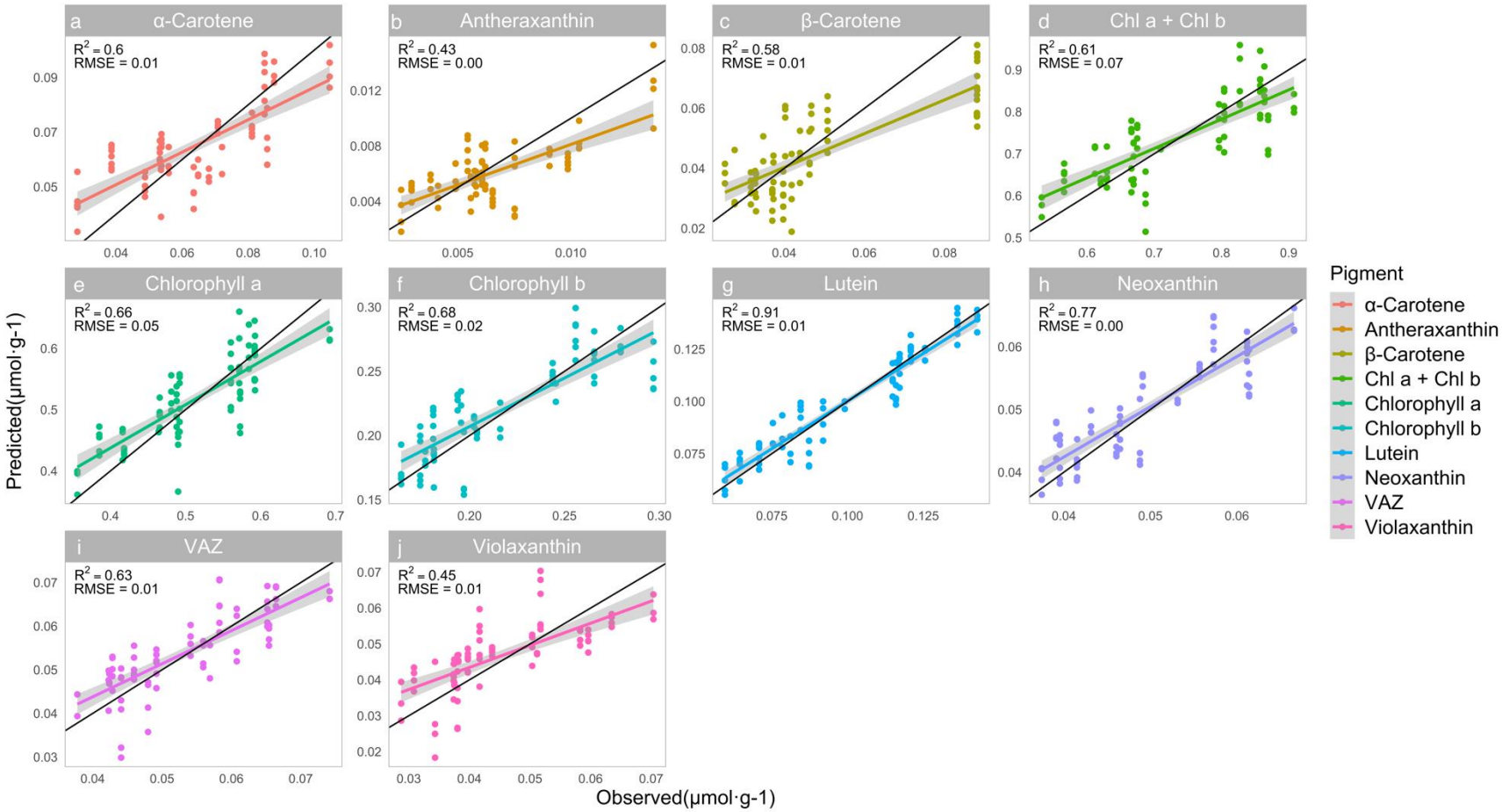

Figure 2.3. Validation results for the chlorophyll and carotenoid pigment/pools predicted from PLSR models using hyperspectral reflectance; from top-left and alphabetically; α-carotene, antheraxanthin, β-carotene, chlorophyll a + chlorophyll b (Chl a + Chl b), chlorophyll a, chlorophyll b, lutein, neoxanthin, violaxanthin + antheraxanthin + zeaxanthin (VAZ), and Violaxanthin. Each pigment has a distinct color depicted in the legend. The coefficient of determination (R^2) line is color-coded with its respective pigment, the shaded gray region is the 95% CI, R^2 and root

mean square error (RMSE) values reported in the top left quadrant of each graph. The solid black line indicates the 1:1 line for observed versus predicted pigment content. All values were found to be significant, with p-values that were all smaller than 10^{-12}.

The variable importance in projection (VIP) metric was calculated to identify the bands within the spectrum that carried the most weight in the individual model calibrations (Fig. 2.4). Generally, the VIP values displayed consistent patterns across all pigments over the entire spectrum; the regions of most importance were in the green, red-edge, and NIR regions (Fig. 2.4). More specifically, wavelengths in the NIR region (around 1400 nm) were important across all pigment/pool predictions, but were more heavily weighted for both α- and β-carotene as well as the pigment pool of V+A+Z and antheraxanthin (Fig. 2.4). The red-edge spectral region was most important for all pigment predictions; it was most influential for the chlorophyll *a* + chlorophyll *b* pool, followed up by chlorophyll *b* individually. Unlike the green, red-edge and NIR regions which were important for pigment prediction across the board, the blue region was selectively important for α-carotene, antheraxanthin, β-carotene, and chlorophyll *a* with VIP values of greater than 1.5. The regression coefficients for all pigments across the whole spectrum are reported in Figure 2.5

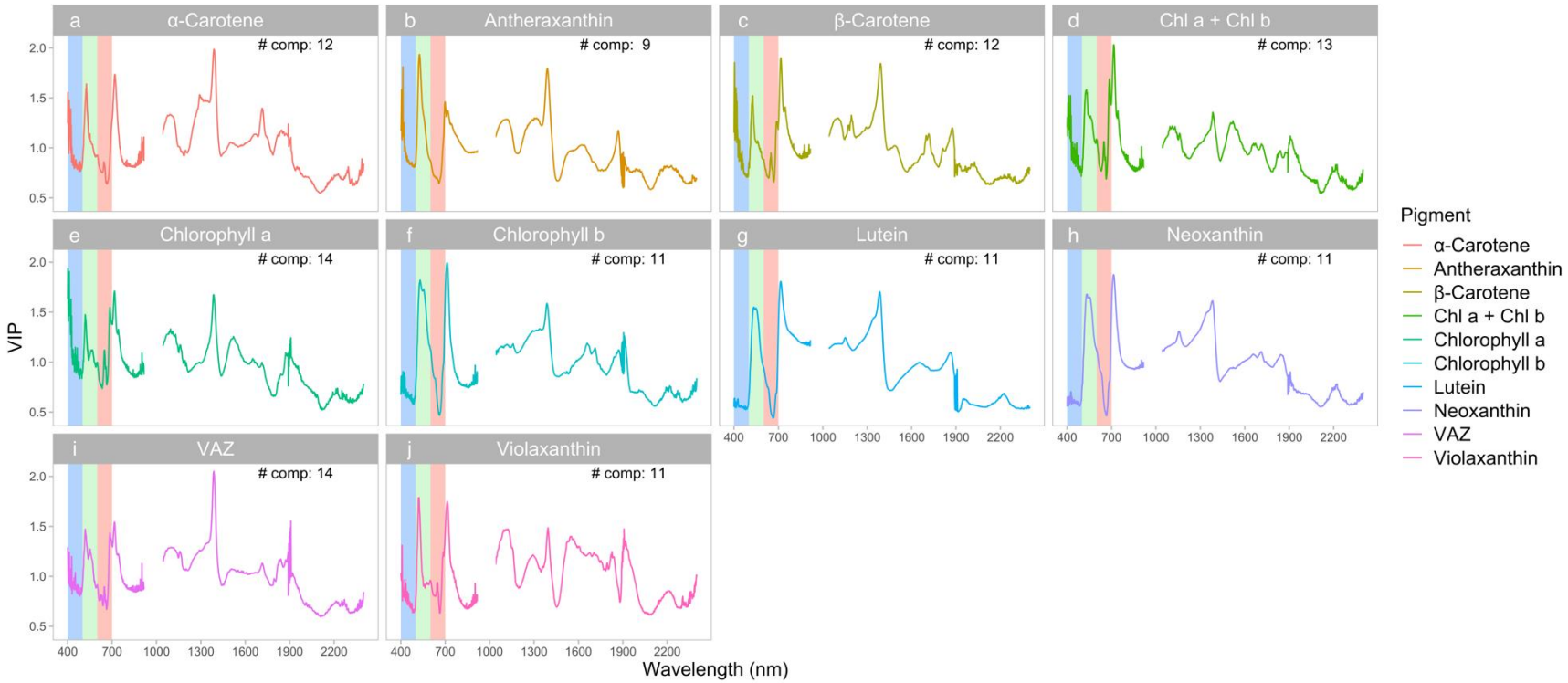

Figure 2.4 Variable importance projection (VIP) results for all pigments/pools across the full spectrum (400 nm - 2400 nm). Visible spectrum regions of blue, green, and red are shaded in their respective wavelengths. The optimal number of components (# comp) included in each PLSR model, individualized for each pigment, is noted in the paragraph.

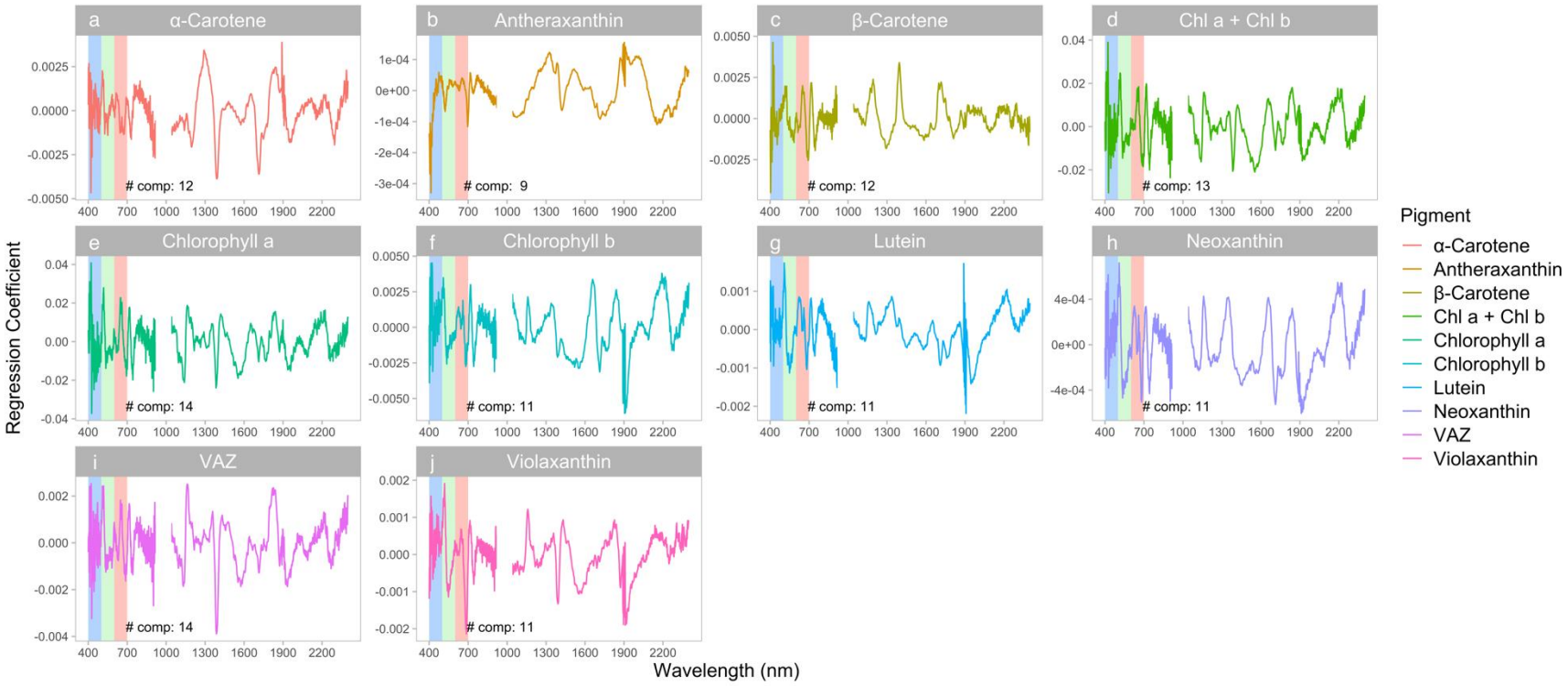

Figure 2.5. Regression coefficient results for all pigments/pools across the full spectrum (400 nm - 2400 nm). Visible spectrum regions of blue, green, and red are shaded in their respective wavelengths. The optimal number of components (# comp) included in each PLSR model, individualized for each pigment, is noted in the graph.

2.5 Discussion

Overall, we successfully utilized PLSR modeling to predict the concentrations of eight individual pigments and two pigment pools in *Pinus palustris* using hyperspectral reflectance measurements at the leaf level. Our results highlight the value of needle mat methodology and leaf-level remote sensing for understanding the physiological status of evergreen species and their underlying pigments. We were best able to predict lutein, neoxanthin and both chlorophylls (Fig. 2.4g-h, d-e, respectively). However, the generally strong predictive performance of the PLSR models, with R^2 values > 50% for eight of the ten pigments/pools, underscores the potential of hyperspectral remote sensing to estimate pigment concentrations with relatively high accuracy (Table 2.1; Fig 2.3).

As expected, and supported by the VIP scores from our PLSR models, the spectral regions of green and red-edge were consistently important for all pigments (Fig. 4). These regions are known for their connection to chlorophyll and carotenoid pigments (Wong and Gamon 2015; Gamon et al. 2016; Wong et al 2020). For instance, Seyednasrollah et al. (2020) emphasizes the sensitivity of chlorophyll and carotenoids in evergreen conifer canopies to seasonal variations, illustrating how these changes directly relate to photochemical processes. Seyednasrollah et al. (2020) discovered that seasonal shifts in canopy color correspond with alterations in the quantum efficiency of PSII photochemistry (Fv/Fm), the Photochemical Reflectance Index (PRI), and consequently changes in leaf pigment pools—particularly chlorophyll and carotenoids, as well as their ratio (chl:car). Furthermore, when exploring the relationship between spectral components,

carotenoid content, and gross primary production, Cheng et al. (2020) determined that the main spectral feature centered around 530 nm was crucial for deducing the seasonal cycle of reflectance-based indices and light use efficiency, corresponding to changes in carotenoid content. Our study encompassed measurements taken across a season (summer, autumn, and winter), thereby incorporating the small, temporal variations in leaf pigment content (Fig. 2.6). This might explain why our PLSR models identified the green, red-edge regions as consistently important. Through addressing the seasonality of these pigments, we can offer a more robust understanding of the connections between spectral measurements, pigment content, photochemical processes, and the environmental factors that influence these changes.

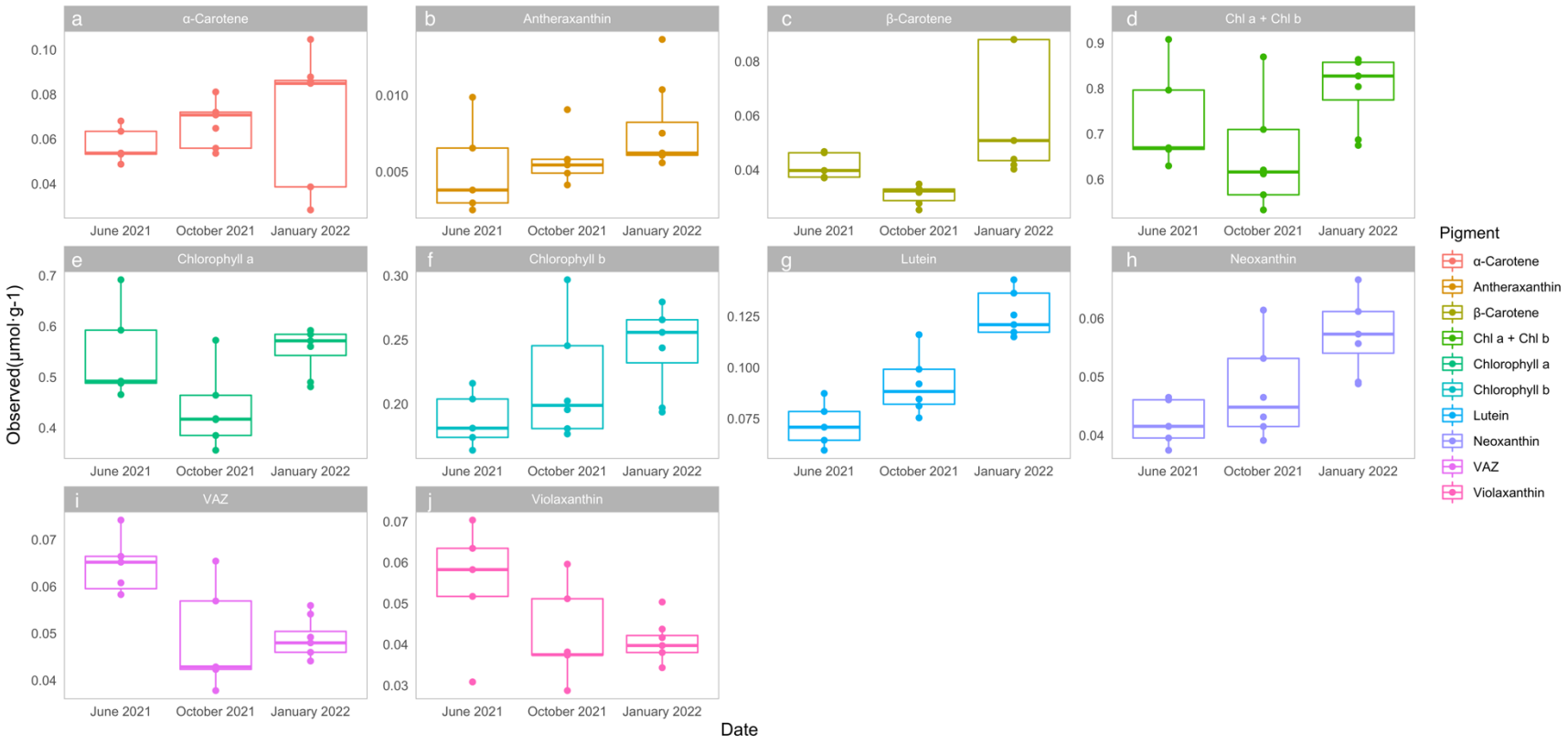

Figure 2.6. Shows the seasonal dynamics of the eight pigments and two pigment pools. Note the varying y-axis for each pigment; from top-left and alphabetically; α-carotene, antheraxanthin, β-carotene, chlorophyll *a* + chlorophyll *b* (Chl a + Chl b), chlorophyll *a,* chlorophyll *b,* lutein, neoxanthin, violaxanthin + antheraxanthin + zeaxanthin (VAZ), and Violaxanthin. Each pigment has a distinct color depicted in the legend that is the same as other figures throughout the paper.

Additionally, the regions around 1200 nm and 1400 nm, which are known regions for water absorption (Curran 1989; Gao 1996; Serbin et al. 2014) were also important for all parameters, although the VIP values tended to be higher for the 1400 nm region (Fig. 2.4). Water plays a crucial role in the photosynthetic process by providing protons and electrons for the light reactions, and its content in leaves can affect pigment concentrations and energy transfer (Kramer, Evanson, and Edwards 2004; Sharma et al. 2020). Therefore, these regions provide valuable information on plant water status and its relationship with pigment dynamics. Similarly, the spectral regions of 1820 nm and 1900 nm, which are important absorption regions for lignin, starch, and cellulose (Curran 1989; Kokaly et al. 2009), were also found to be important for most pigments (Fig. 2.4). Changes in the absorption properties of these regions can indicate variations in leaf structural properties that may influence pigment concentrations and photosynthetic processes. The importance of these spectral regions in predicting pigment concentrations emphasizes the value of hyperspectral remote sensing for understanding plant physiology. By capturing the unique absorption features of different pigments, hyperspectral data enables researchers to estimate pigment concentrations and gain insights into the complex relationships between pigments, photosynthesis, and plant health.

The strong predictive performance of the PLSR models demonstrated here indicates that hyperspectral remote sensing can be a valuable tool for monitoring pigment concentrations in evergreen species such as *Pinus palustris*. These findings are particularly relevant in the context of recent advancements in remote sensing technology (such as the hyperspectral missions NASA SBG and AVIRIS-NG). Thus, enabling researchers to capture fine-scale information on pigment

dynamics across diverse ecosystems and environmental gradients, these missions hold great promise for improving our understanding of relating remote sensing measurements to plant physiology.

2.6 References

Askari MS, McCarthy T, Magee A, Murphy DJ. **2019**. Evaluation of grass quality under different soil management scenarios using remote sensing techniques. *Remote Sensing* **11**: 1–23.

Badgley G, Field CB, Berry JA. **2017**. Canopy near-infrared reflectance and terrestrial photosynthesis. *Science Advances* **3**: 1–6.

Blackburn GA. **2007**. Hyperspectral remote sensing of plant pigments. *Journal of Experimental Botany* **58**: 855–867.

Bowling DR, Logan BA, Hufkens K, *et al.* 2018. Limitations to winter and spring photosynthesis of a Rocky Mountain subalpine forest. *Agricultural and Forest Meteorology* **252**: 241–255.

Burnett AC, Anderson J, Davidson KJ, *et al.* 2021. A best-practice guide to predicting plant traits from leaf-level hyperspectral data using partial least squares regression. *Journal of Experimental Botany* **72**: 6175–6189.

Cazzonelli CI. **2011**. Carotenoids in nature: Insights from plants and beyond. *Functional Plant Biology* **38**: 833–847.

Cawse-Nicholson K, Raiho AM, Thompson DR, *et al.* 2023. Surface Biology and Geology imaging spectrometer: A case study to optimize the mission design using intrinsic dimensionality. *Remote Sensing of Environment* **290**: 113534.

Curran PJ. **1989**. Remote sensing of foliar chemistry. *Remote Sensing of Environment* **30**: 271–278.

Dall'Osto L, Cazzaniga S, North H, Marion-Poll A, Bassia R. **2007**. The Arabidopsis aba4-1 mutant reveals a specific function for neoxanthin in protection against photooxidative stress. *Plant Cell* **19**: 1048–1064.

Demmig-Adams B, Adams WW. **2006**. Photoprotection in an ecological context: The remarkable complexity of thermal energy dissipation. *New Phytologist* **172**: 11–21.

Demmig-Adams B, Adams WW. **1996**. The role of xanthophyll cycle carotenoids in the protection of photosynthesis. *Trends in Plant Science* **1**: 21–26.

Gamon JA, Field CB, Bilger W, Björkman O, Fredeen AL, Peñuelas J. **1990**. Remote sensing of the xanthophyll cycle and chlorophyll fluorescence in sunflower leaves and canopies. *Oecologia* **85**: 1–7.

Gamon JA, Huemmrich KF, Wong CYS, *et al.* 2016. A remotely sensed pigment index reveals photosynthetic phenology in evergreen conifers. *Proceedings of the National Academy of Sciences of the United States of America* **113**: 13087–13092.

Gamon JA, Penuelas J, Field CB. **1992**. A Narrow-Waveband Spectral Index That Tracks Diurnal Changes in Photosynthetic Efficiency*. *Remote Sensing of Environment* **41**: 35–44.**Gao B**. **1996**. NDWI—A normalized difference water index for remote sensing of vegetation liquid water from space. *Remote Sensing of Environment* **58**: 257–266.

Garbulsky MF, Peñuelas J, Gamon J, Inoue Y, Filella I. **2011**. The photochemical reflectance index (PRI) and the remote sensing of leaf, canopy and ecosystem radiation use efficiencies. A review and meta-analysis. *Remote Sensing of Environment* **115**: 281–297.

Geladi P, Kowalski BR. **1986**. Partial least-squares regression: a tutorial. *Analytica Chimica Acta* **185**: 1–17.

Giossi C, Cartaxana P, Cruz S. **2020**. Photoprotective role of neoxanthin in plants and algae. *Molecules* **25**.

Gitelson AA, Gritz Y, Merzlyak MN. **2003**. Relationships between leaf chlorophyll content and spectral reflectance and algorithms for non-destructive chlorophyll assessment in higher plant leaves. *Journal of Plant Physiology* **160**: 271–282.

Gitelson AA, Merzlyak MN. **1996**. Signature analysis of leaf reflectance spectra: Algorithm development for remote sensing of chlorophyll. *Journal of Plant Physiology* **148**: 494–500.

He P, Xu X, Zhang B, *et al.* 2015. Estimation of leaf chlorophyll content in winter wheat using variable importance for projection (VIP) with hyperspectral data. *Remote Sensing for Agriculture, Ecosystems, and Hydrology XVII* **9637**: 963708.

Helm LT, Shi H, Manuel LT, Yang X. **2020**. Solar-induced chlorophyll fluorescence and short-term photosynthetic response to drought. *Ecological Applications* **30**: 1–12.

Huang J, Wei Chen, Zhang Y, *et al.* 2015. Meta-analysis of the detection of plant pigment concentrations using hyperspectral remotely sensed data. *PLoS ONE* **10**: 1–26.

Jahns P, Holzwarth AR. **2012**. The role of the xanthophyll cycle and of lutein in photoprotection of photosystem II. *Biochimica et Biophysica Acta - Bioenergetics* **1817**: 182–193.

Kira O, Linker R, Gitelson A. **2015**. Non-destructive estimation of foliar chlorophyll and carotenoid contents: Focus on informative spectral bands. *International Journal of Applied Earth Observation and Geoinformation* **38**: 251–260.

Kokaly RF, Asner GP, Ollinger S V., Martin ME, Wessman CA. **2009**. Characterizing canopy biochemistry from imaging spectroscopy and its application to ecosystem studies. *Remote Sensing of Environment* **113**: S78–S91.

Kramer DM, Avenson TJ, Edwards GE. **2004**. Dynamic flexibility in the light reactions of photosynthesis governed by both electron and proton transfer reactions. *Trends in Plant Science* **9**: 349–357.

Mevik B-H, Wehrens R. **2007.** The PLS package: Principal component and partial least squares regression in R. *J Stat Softw*. 2007;**1**(2).

Lu C, Lu Q, Zhang J, Kuang T. **2001**. Characterization of photosynthetic pigment composition, photosystem II photochemistry and thermal energy dissipation during leaf senescence of wheat plants grown in the field. *Journal of Experimental Botany* **52**: 1805–1810.

Magney TS, Bowling DR, Logan BA, *et al.* 2019. Mechanistic evidence for tracking the seasonality of photosynthesis with solar-induced fluorescence. *Proceedings of the National Academy of Sciences of the United States of America* **116**: 11640–11645.

Magney TS, Vierling LA, Eitel JUH, Huggins DR, Garrity SR. **2016**. Response of high frequency Photochemical Reflectance Index (PRI) measurements to environmental conditions in wheat. *Remote Sensing of Environment* **173**: 84–97.

Mahajan GR, Das B, Murgaokar D, *et al.* 2021. Monitoring the foliar nutrients status of mango using spectroscopy-based spectral indices and plsr-combined machine learning models. *Remote Sensing* **13**: 1–24.

Melkozernov, A.N., Blankenship, R.E. (2006). Photosynthetic Functions of Chlorophylls. In: Grimm, B., Porra, R.J., Rüdiger, W., Scheer, H. (eds) Chlorophylls and Bacteriochlorophylls. Advances in Photosynthesis and Respiration, Vol 25. Springer, Dordrecht.

Palta JP. **1990**. Leaf chlorophyll content. *Remote Sensing Reviews* **5**: 207–213.

Porcar-Castell A, Tyystjärvi E, Atherton J, *et al.* 2014. Linking chlorophyll a fluorescence to photosynthesis for remote sensing applications: Mechanisms and challenges. *Journal of Experimental Botany* **65**: 4065–4095.

Porcar-Castell A, Malenovský Z, Magney T, *et al.* 2021. Chlorophyll a fluorescence illuminates a path connecting plant molecular biology to Earth-system science. *Nature Plants* **7**: 998–1009.

Rajewicz PA, Atherton J, Alonso L, Porcar-Castell A. **2019**. Leaf-level spectral fluorescence measurements: Comparing methodologies for broadleaves and needles. *Remote Sensing* **11**.

Schimel D, Schneider FD. **2019**. Flux towers in the sky: global ecology from space. *New Phytologist* **224**: 570–584.

Serbin SP, Dillaway DN, Kruger EL, Townsend PA. **2012**. Leaf optical properties reflect variation in photosynthetic metabolism and its sensitivity to temperature. *Journal of Experimental Botany* **63**: 489–502.

Serbin SP, Singh A, McNeil BE, Kingdon CC, Townsend PA. **2014**. Spectroscopic determination of leaf morphological and biochemical traits for northern temperate and boreal tree species. *Ecological Applications* **24**: 1651–1669.

Sharma A, Kumar V, Shahzad B, *et al.* 2020. Photosynthetic Response of Plants Under Different Abiotic Stresses: A Review. *Journal of Plant Growth Regulation* **39**: 509–531.

Sims DA, Gamon JA. **2002**. Relationships between leaf pigment content and spectral reflectance across a wide range of species, leaf structures and developmental stages. *Remote Sensing of Environment* **81**: 337–354.

Smith ML, Ollinger S V., Martin ME, Aber JD, Hallett RA, Goodale CL. **2002**. Direct estimation of aboveground forest productivity through hyperspectral remote sensing of canopy nitrogen. *Ecological Applications* **12**: 1286–1302.

Steidle Neto AJ, Moura L de O, Lopes D de C, Carlos L de A, Martins LM, Ferraz L de CL. **2016**. Non-destructive prediction of pigment content in lettuce based on visible-NIR spectroscopy. *Journal of the Science of Food and Agriculture* **97**: 2015–2022.

Thompson DR, Guanter L, Berk A, *et al.* 2019. Retrieval of Atmospheric Parameters and Surface Reflectance from Visible and Shortwave Infrared Imaging Spectroscopy Data. *Surveys in Geophysics* **40**: 333–360.

Tucker CJ. **1979**. Red and photographic infrared linear combinations for monitoring vegetation. *Remote Sensing of Environment* **8**: 127–150.

Ustin SL, Gitelson AA, Jacquemoud S, *et al.* 2009. Retrieval of foliar information about plant pigment systems from high resolution spectroscopy. *Remote Sensing of Environment* **113**: S67–S77.

Wold S, Ruhe A, Wold H, Dunn, III WJ. **1984**. The Collinearity Problem in Linear Regression. The Partial Least Squares (PLS) Approach to Generalized Inverses. *SIAM Journal on Scientific and Statistical Computing* **5**: 735–743.

Wold S, Sjöström M, Eriksson L. **2001**. PLS-regression: A basic tool of chemometrics. *Chemometrics and Intelligent Laboratory Systems* **58**: 109–130.

Wolter PT, Townsend PA, Sturtevant BR, Kingdon CC. **2008**. Remote sensing of the distribution and abundance of host species for spruce budworm in Northern Minnesota and Ontario. *Remote Sensing of Environment* **112**: 3971–3982.

Wong CYS, D'Odorico P, Arain MA, Ensminger I. **2020**. Tracking the phenology of photosynthesis using carotenoid-sensitive and near-infrared reflectance vegetation indices in a temperate evergreen and mixed deciduous forest. *New Phytologist* **226**: 1682–1695.

Wong CYS, Gamon JA. **2015**. Three causes of variation in the photochemical reflectance index (PRI) in evergreen conifers. *New Phytologist* **206**: 187–195.

Wong CY, Gilbert ME, Pierce MA, *et al.* 2023. Hyperspectral Remote Sensing for Phenotyping the Physiological Drought Response of Common and Tepary Bean. *Plant Phenomics* **5**: 1–11.

Xue L, Yang L. **2009**. Deriving leaf chlorophyll content of green-leafy vegetables from hyperspectral reflectance. *ISPRS Journal of Photogrammetry and Remote Sensing* **64**: 97–106.